Master Thesis
SIMaP Laboratoire, CNRS

Τμήμα Φυσικής, Πανεπιστήμιο Κρήτης, Ελλάδα
Institute Polytechnique de Grenoble, Université Grenoble-Alpes, France

June 2022

Polycrystalline SiC for brain implantable electrodes

Michalis Gavalas

Polycrystalline SiC for brain implantable electrodes

by

Michalis Gavalas

Master thesis
Master of Physics in Photonics and Nanoelectronics
and
«SICNeural» scientific program of French ANR.
Department of Physics, UoC
and
Grenoble INP-UGA

Supervisor: Konstantinos Zekentes, Ph.D
Co-supervisor: Frederic Mercier, Ph.D
University professor: George Deligeorgis, Ph.D

Dedication

To my family

For the endless help in my life

Acknowledgment

On top of the accomplishment of this thesis I would like to give my biggest gratitude to many people that contribute to this success. My first gratitude should be given on the SIMaP laboratory of Grenoble-INP. I would like to thank my supervisor Frederic Mercier, which he was the one that introduce me and gave me the chance to work to his lab, where I met a lot of interesting, highly educated and hard working people. His leadership and guidance throughout the whole period of the thesis, gave me the inspiration and the willing of never stop trying, with a lot of his useful and important advices, on how to be efficient and productive in my work.

I could give further gratitude to Elisabeth Blanquet, director of SIMaP laboratory for the big opportunity she also gave me to work on this lab and the FORTH researcher Konstantinos Zekentes, who gave me the chance to be part of a scientific program by ANR and collaborating with many important and well-known research groups throughout France.

Many thanks should be also given to my colleague, Ph.D student Jorge S. Espinoza. Jorge was the one that took care of my experimental training and the introduction to the main functions of the laboratory. He was always there and never hesitated to help me with my experimental confusion, pausing his own work, even for just a few moments. Something that is really invaluable.

Next, I give many thanks to my fellow researcher Clement Hebert, which he gave me the opportunity to work on his lab. He was always giving me useful advices as well, on how to be precise and thinking outside the box, while I'm facing a very confusing problem. We exchange many times ideas on how to develop and be more productive, something that helped me a lot during my research and experimenting period.

I would like also to thank Alexander Crisci. As the technician of the SIMaP Lab, he took care of my first step of training in many scientific instruments and characterizing methods. He also help me a lot with the experimental procedures of many characterizing procedures.

Many thanks also should give on Francine and Joelle. These two researchers gave me the chance to train and use their facilities for many experimental observations on their equipment. Both of them were really nice and patient with me and always pointed me how significant it is to be calm and focus, even when the experiment has a lot of difficulties on the way.

Beyond the SIMaP I would like to thank all of my close friends here in Grenoble, with those I learned and explore the city and the daily life on this part of France. I give also many thanks to my close friends in Greece, which they wanted to learn always news from me and here about my life changing, my progress and my future plans about my life.

Outline Table

Abstract

Silicon carbide (SiC) technology has come to a big interest the last years in research community mainly due to its suitability for high power applications. Nowadays SiC has also high attendance, due to its biocompatibility with organic tissue, for bio-medical research and applications and also for construction of neural interfaces electronic brain chips and micro-electrode arrays (MEAs).

The present thesis deals with the growth of polycrystalline SiC thin films with Low Pressure Chemical Vapor Deposition (LPCVD) for neural interfaces applications. The study is focusing on low temperature growth below the 1200^{o}C with the use of a cold-wall reactor. In situ doping of the thin films is achieved with ammonia. The deposition is performed on silicon wafers. In situ chloride treatment during the synthesis is shown to be important for the modulation of the deposition rate and overall grown thickness of the deposited thin film. Additionally, we show that dichloride gas also affects the grain size and the overall surface morphology of the film.

The grown material is examined by structural, mechanical and electrical characterization methods to determine the grown thickness, crystallinity, surface morphology, residual stress, electrical resistivity and electrochemical charge storage capacity. Microscopic structure is shown to deeply affect the macroscopic properties of the deposited films. Overall characterization shows that the polycrystalline SiC thin films can be able to work properly as the active material for recording-stimulating neural interface.

Keywords: Low pressure chemical vapor deposition, polycrystalline SiC, n-doping, design of experiment, cyclic voltammetry, electrochemical impedance spectroscopy, brain implantable electrodes, neural interfaces

List of abbreviations

BMI: Brain Machine Interface

BCI: Brain Computer Interface

CNS: Central Nervous system

PNS: Peripheral Nervous system

SiC: Silicon carbide

MEAs: Microelectrode arrays

AP: Action Potential

EGG: Electroencephalography

ECoG: Electrocorticography

MEMS: Micro-electromechanical systems

CVD: Chemical Vapor Deposition

SEM: Scanning Electron Microscopy

CV: Cyclic Voltammetry

CSC: Charge Storage Capacity

CD: Charge Delivery

EIS: Electrochemical Impedance Spectroscopy

DOE: Design of Experiment

PBS: Phosphate Buffer Solution

XRD: X-ray Diffraction

AC: Alternative current

Sccm: standard cubic centimeter per minute

Motivation of Work

Brain machine interfaces (BMIs) technology emerges in order to give medical solutions in patients that express neural disorders of the central nervous system (CNS) or the peripheral nervous system (PNS), or suffer from lost functions or neural traumas ([1]). Brain implantable electrodes have been proven promising for neural recording and stimulation. Their steady and efficient performance along with their long-term biocompatibility is very important for neural prostheses.

Neural electrodes have been demonstrated with various options of materials that could be promising as reliable active recording/stimulating site. So far, various semiconductor and polymer based devices, have been developed towards this purpose. For instance PEDOT:PSS seems to dominate compare to other polymer choices and overall in the electrochemical performance for capable neural stimulation (CSC ~ 50 mC/cm^2) ([2], 2009). Very thin wires of PEDOT:PSS are capable to mimic the neural shape, limiting as much as possible the foreign body response. However micromotions based on the mechanical interface between the polymer and the neural tissue, show miss-orientations of the neural probes that result to false neural recording ([6]). Semiconductors like Si have also been reported as capable based material for micro electrode array devices fabrication. The Utah electrode array and the Michigan electrode are prime examples of Si based electrodes, with low electrochemical impedance (~50kΩ at 1 kHz) ([4]). However Si based device suffer from mechanical mismatches mostly in chronic in-vivo use, due to Si mechanical properties.

Previous in-vivo and in-vitro studies have shown that silicon carbide (SiC) is a suitable material for biomedical devices. In fact, SiC is a semiconductor that is chemically inert and presents high biocompatibility. Mechanically it shows high toughness, which is 5 times higher than the pure Si and better bulking characteristics, something that makes it capable for flexible and thin device fabrication reducing the overall biotic response. Many cases present the epitaxial and polycrystalline form of SiC as suitable materials for active neural recording.

Polycrystalline SiC has been many times reported as a capable material for MEMS applications. N-doped poly-SiC can reach sheet resistivity as low as some mΩ*cm ([5]). The residual stress can also be modulated depending of the synthesis process ([3]). Since it maintains its biocompatibility independent of the doping and mechanical modulation, biomedical devices can be developed based on poly-SiC. With low electrochemical impedance, below 100kΩat 1 kHz, microelectrode arrays can be successfully fabricated for active neural recording and stimulation ([7]). It has been show that cubic polycrystalline SiC (3C-poly-SiC) can successfully compete with its epitaxial counterpart, in terms of electrochemical performance, as long as it can provide an electrochemical water window as wide as 2V and steady capacitive currents of 6μA, which outruns the epitaxial counterpart performance by some orders of magnitude (~50nA for 4H-SiC epitaxial) ([8]), ([9]). Based on this state of art, we present the deposition of polycrystalline SiC thin films and their characterization as highly suitable films for promising neural recording and stimulation interfaces.

Chapter 1: Introduction

1.1 Brain Computer Interface

Brain Computer Interfaces (BCIs) is a vast scientific and technological domain that shows great interest in the last 40 years of science. The idea is occurred through the direct bonding of a pure digital computer with the central nervous system or the peripheral nervous system. By definition the BCI is a system that records the CNS or PNS activity and is able to translate it in suitable electrical signal through the recording technology, which is going to be analyzed or modified by an electronic computing system ([10]). Many attempts have been done to receive neural recording outputs and translate them within a computer to motor outputs of a mechanical part ([11]). The signals are usually recorded by using sensors on the scalp surface of the brain or electrodes implanted inside the scalp within the brain itself of the patient, interfacing directly the neurons ([12]).

BCI's ultimate goal is to enable directly connection and communication between the live conscious brain and the electronic machine or computer, with the ability of adaption and work production or information exchange during the communication procedure. Medical reasons are the most common examples taking into account patients that suffer from Parkinson's decease or have suffer traumatic spinal cord injury.BCI could restore or even replace a muscle motor control output that lost within an injury or decease and even allow the speaking function that was terminated by a brainstem stroke ([15]). Other useful applications are on the rise like the ability of supply and improve the natural output signals of the CNS, in terms of remote controlling a robotic arm only by consciousness or enhancement of the alarming conditions during a driving session.

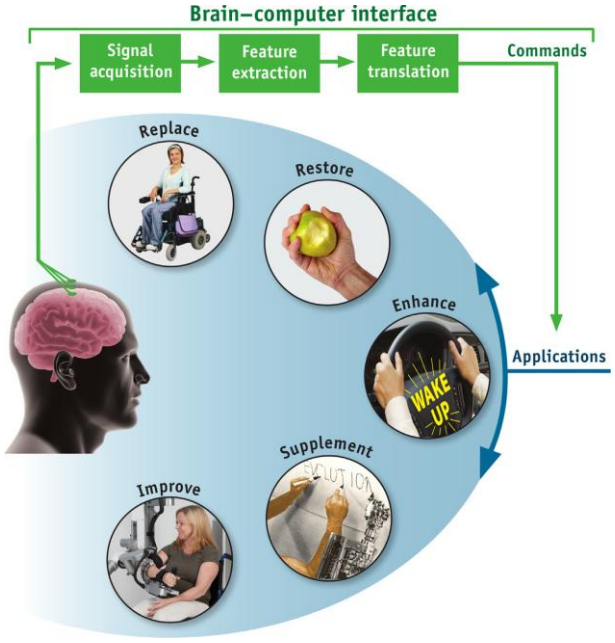

Figure 1.1.1. Brain Computer Interface applications. Electrical or other signal reflecting the brain activity are recorded from the scalp the cortical phase or within the brain. They are analyzed to measure signal features that indicate the BCI user's inert. These features are able to be translated into commands for an operating application like, muscle motor output or neural enhancement and many more ([15]).

1.2 Neural Interfaces

«Neural interfaces» is the primary evolving research domain of the BCI systems the recent scientific years. Based on the rise of the microelectronics and materials science and technology the modern neural interfaces have a huge role on the advanced BCI systems and their applications. The average neuro-tech research community focuses on the advance and the development new microelectronic devices also with high biocompatibility to improve the neural signal recording and minimize the medical issues that may occur on the process like the inflammatory effects and the glial scars, when the interface is succeeded.

The microelectronic implanted electrodes are made with promise to limit the signal-to-noise ratio (SNR) from several individual neurons, receiving their action potentials (APs) ([13]). For this reason, the microelectrode arrays (MEAs) type of neural interfaces have been dominating the last years. The *in vivo* electrodes are divided by their position at the time of their signal recording. In general, the electrodes that are brain implanted tend to have lesser SNR than the ones used in the electroencephalography (EEG) method and are classified according to the method used to fabricate the probe that will be detecting the neuron's action potential. The material's technology is an important domain in the fabrication process, focusing mostly on flexibility and elasticity for the smooth functionality on the implanted electrode. In terms of biocompatibility many choices have risen the last years such fabricating titanium based and polymeric based electrodes, although it is not clear which one has better chance of avoiding extensive inflammatory and glial scar on the scalp.

Device	Invasive	Long-Term Reliability (days)	Advantages	Disadvantages
Utah Electrode Array	Yes	502	Small impedance	Micro-cracks in *in vivo* chronic use
Platinum Stent Electrode	No	190	Steady endovascular recording	Minimal invasiveness
Neuron-like Electrode	Yes	90	Minimizes the foreign body response	Micro-movements can result in false recording
PEG: Tetrode	Yes	-	Small impedance	-
PEDOT:PSS-CNT	Yes	30	High capability of neural stimulation	Polymer aging leads to mechanical mismatches
Au wires	Yes	-	Small impedance	Poor neural stimulation
All-SiC	Yes	-	High biocompatibility and good capacitive behavior	-

Table 1.2.1. Summary of Neural probes devices and their properties on *in-vivo* applications.

Micro electrode arrays like the Utah electrode and the Michigan were the first fabricated devices displaying electrochemical impedance of 150kΩat 1 kHz ([4]). However the electrode can suffer from many mechanical failures in an *in-vivo* chronic use ([14]). Another case showed that platinum based endovascular stent electrodes tend to minimize the invasiveness while maintain the biocompatibility and the long-term reliability ([15]). Although they can provide steady recording, due to the limited invasive level, the recorded signal is poor and not selective, like most of the implantable MEAs. Platinum-based

electrodes coated with conductive polymer, Neuron-like electrodes have been also demonstrated. These electrodes tend to mimic the neuron physiology in terms of thickness and shape, in order to minimize as much as possible the foreign body response ([6]). Although they can have multi neuron recording simultaneously, micro motions were occurred after 90 days of implantation, failing to acquire steady signal from the desired region of neuron. Similar study has shown that carbon nanotubes or PEG coated tetrode electrodes display electrochemical impedance as low as 30kΩ at 1 kHz ([16]). Tetrode electrodes are constructed by bundling together four very small wire-like electrodes. Usually are used for applying a small extra cellular field potential.

Silicon carbide based devices have been also reported many times as promising neural interfaces combining the desired electrical and mechanical properties for an invasive operation with satisfying recording and stimulating properties.

1.3 Silicon-Carbide in Neural technology

It has been reported many times that silicon carbide (SiC) has been used as a based material for the fabrication of neural interfaces ([7]), ([17]), ([18]). Silicon carbide is a semiconductor that has been proven to be highly biocompatible and chemically inert, that promises long-term reliability ([17]). The cubic form, 3C-SiC has shown utility as a material for micro-electromechanical systems (MEMs). Additional *in-vitro* and *in-vivo* studies have been reported promising demonstration of epitaxial 3C-SiC for increased levels of neural acceptability ([17]), ([18]). The amorphous also counterpart of SiC has been proved highly accepted insulating coating for neural devices as it is proved also highly compatible in the neural ambience ([7]).

In vivo studies of epitaxial 3C-SiC neural probes in mice's brains have reported significant less immune response compare to its counterpart pure epitaxial Si material. The first attempt for their long term reliability has been reported also that after 35 days of implantation into the midbrain of the mice, the epitaxial 3C-SiC probes showed very limited microglia and macrophage activity compare to the pure epitaxial Si probes ([18]). Also the tissue voids by immunofluorescence, surrounding the 3C-SiC probe, that had been observed were much smaller in size in contrast with the Si ones. Recent studies have been shown that another polytype, the tetrahedral form, 4H-SiC is suitable based material for the development of more complex neural devices ([19]). The devices showed electrochemical impedance profile Z of 800 kΩ at 1kHz ([19]). Another all-SiC with epitaxial 4H-SiC recording sites displayed impedance range of 46.5kΩ-675kΩ at 1 kHz, and a charge storage capacity of almost 5 $\mu C/cm^2$ ([20]).

Silicon carbide neural interfaces with polycrystalline 3C-SiC recording sites have been developed ([7]). Diaz et al. has exhibited a new array device of neural probe with polycrystalline silicon carbide as electrode recording sites for ECoG reasons ([7]). Polycrystalline n-SiC is used as the recording site. The doped film is presenting resistivity of nearly 2 mΩ*cm, while the fabricated microelectrodes shows electrochemical impedance as low as 36kΩ at 1 KHz, after platinum black electroplating.

Overall the epitaxial 4H-SiC and polycrystalline 3C-SiC based microelectrodes, show to match the electrochemical impedance performance of polyimide coated Si (Utah electrode

array) and the PEDOT:PSS based microelectrodes. However their capacitive performance tends to be significant lower compare to the conductive polymeric materials. Table 1.3.1 displays the electrical and electrochemical properties of various materials, related with microelectrode devices.

For neural probes applications, the full electrical and electrochemical output maybe differ based on the dimensional scale of active surface area of the material. In terms of charge storage and impedance the performance is directly associated with the available exposed electrochemical active area. For example impedance values are significantly increased from large geometrical surface areas (GSA) to small ones. On the other hand the capacitive performance is more complex, as it is associated with the surface quality, in terms of roughness and surface defects. Electrical sheet resistivity is not directly associated directly with electrochemical capacitive performance, although conductive materials are always part in microelectrode devices. In most cases the desired based material for a fabricated microelectrode device, presents metallic or semi-metallic behavior. The need for a conductive line and good ohmic contacts results in employing metals and doped semiconductors, while conductive polymers are usually used for coating the recording site.

Material/Device	Charge Storage Capacity (mC/cm^2)	Charge Injection Mechanism	Resistivity (Ω*cm)	Impedance (kΩ @ 1kHz)	Electrolyte	Voltage (V)
Si-Polyimide (Utah Electrode)	-	Faradaic/Capacitive	-	80-150	PBS	-
Parylene C	-	Faradaic/Capacitive	$8.8*10^{16}$	2000	PBS	-
Pt	$54\text{-}150*10^{-3}$	Faradaic/Capacitive	$10.6*10^{-6}$	-	PBS	-0.7-0.7
Au	$110*10^{-3}$	Faradaic/Capacitive	$2.5*10^{-8}$	-	0.1M KCL	-0.6-0.8
PEDOT:PSS	75	Faradaic	0.02	23.3-442	PBS/Ringer's	-0.9-0.6
3C-SiC epitaxial	-	Capacitive	0.14	~800	PBS	-
4H-SiC epitaxial	$4.38*10^{-3}$	Capacitive	-	46.5-675	PBS	-2.0-2.8
IrO_2	28	Faradaic/Capacitive	$42.6*10^{-6}$	113.6	PBS	-0.8-0.8
TiN	2-3.3	Capacitive	0.005	43-94	PBS	-0.9-0.9
N-type Polycrystalline SiC	-	Capacitive	0.02	~36 (Platinum black electroplating)	PBS	-

Table 1.3.1. Comparison of the electrical and electrochemical properties on various materials for neural interface applications. The displayed values are based on the microelectrode scale device approach (~μm^2), rather than simple material scale (~cm^2). Values on the full material scale maybe differ from these.

1.4. Chemical Vapor Deposition of polycrystalline Silicon Carbide thin films

Polycrystalline SiC deposition has been studied multiple times with low pressure chemical vapor deposition. Table 1.4.1 summarizes the mainstream properties of poly-SiC for microelectromechanical (MEMs) applications. Since the previous research on poly-SiC neural interfaces is limited, here we present the state of art for the parameters and their effect on the main polycrystalline SiC properties for well studied MEMs devices.

Silicon Carbide Property	Typical	Range	Parameter	Effect	Typical	Range
Thickness	2μm	0.1-20μm	C/Si	Determines deposition stoichiometry	2	1-7
			Cl/Si	Chloride prevents poly-Si formation	2	0-4
			N/Si	N-doping Reduces Crystallinity	0.02	0.01-0.05
			Temperature (^oC)	Deposition rate proportional to temperature	900	800-1300
Residual Stress σ	300-600MPa	-(100)-1400 MPa	C/Si	Excess Si decreases the residual stress	2	1-7
			Cl/Si	Surface Etching Surface Roughness Modulation	2	0-4
			N/Si	Over embedded nitrogen increases the stress	0.02	0.01-0.05
			Temperature (^oC)	Depot. Rate is reverse proportional to stress	900	800-1300
Resistivity ρ	1000 Ω*cm	1-10000 Ω*cm	C/Si	Excess Si decreases resistivity	2	1-7
			Cl/Si	Excess chloride lowers resistivity	-	0-4
			N/Si	Performs N-doping	0.02	0.01-0.05
			Temperature (^oC)	Ambient temperature Influence • grain size • crystallinity	900	800-1300

Table 1.4.1. Summary of properties of polycrystalline SiC thin films used for MEAMs applications as a function of growth parameters.

Polycrystalline SiC layers can be grown with LPCVD technique with either hot-wall or cold wall reactors. The usual ambience temperature is arranged between 800^{o}C – 1200^{o}C and the pressure is usually between 100 – 1 mbar. Deposition rate is shown to increasing with temperature. Substrates such as epitaxial silicon, Si(100) or SiO_2/Si show similar results in terms of deposition rate and deposited thickness ([3]).

Chloride ambience was found out to affect the surface conditions of the deposited film. Inducing Cl species either by an accompanied gas or directly by a precursor, polysilicon deposition sites are avoided, as Si-Cl bond is more stable and energetically favorable than the Si-Si chemical bond, and the surface roughness is modulated ([23]). High amount of chloride may be reasonable for a local surface etching, resulting in smoother film surface in the temperature range of 800^{o}C – 1200^{o}C. Thus the selected amount of chloride during deposition can have a significant impact on the average surface roughness of the deposited thin film.

The residual stress of the film can be modulated by the deposition rate as it was reported a change from highly tensile to compressive, for an increasing deposition rate, which is directly associated with the increase in the flow rate of the precursors ([3]). Supplied gas

ratios are proved to affect the residual stress. Stress reduction has been observed in Si-rich layers due to the larger atomic radius of the Si compare to carbon ([3]), ([5]). Since Si has bigger atomic radius excess silicon leads to bigger average bond length and in an overall decrease of the stress. In n-doped SiC films the induced nitrogen tends to lower the crystallinity of the film itself, forming more amorphous-like regions around the doping sites that are responsible for an increase in the residual stress. Thus the N/Si is expected to increase with the residual stress, in contrast with the C/Si ratio, which has been proven that silicon rich film are showing increased residual stress ([5]).As the deposition rate is increased the residual stress changed from highly tensile to near compressive. Especially near the tensile to compressive transition range, a small change in the deposition rate results in a significant change of in the residual stress of the films, both in magnitude and in sign.

Nitrogen performs n-doping to the polycrystalline SiC thin film, as giving an excess electron to the system with each nitrogen atom that it is induced into the SiC lattice. Considerably, the nitrogen atoms can occupy either the Si or C atoms sites with the almost the same efficiency. It is also common for nearly ceramic materials such as SiC to occupy, vacant sites (defects of the crystal) inside the lattice, rather than just to replace any of the silicon or carbon sites. It has been shown that ammonia is a good provider of nitrogen in the range of $800^{o}C - 1200^{o}C$ for *in situ* doping of the deposited polycrystalline SiC thin film ([5]) ([21]). The doping procedure is performed in order to decrease the resistivity.

It has been reported that the typical electrical resistivity of the polycrystalline n-doped SiC with nitrogen atoms can decreased below 1 Ω*cm ([5]). However heavy doping is usually avoided, as the nitrogen induction showed a decrease in the average lattice constant and a reduction to the overall crystallinity of the thin film, forming more amorphous like regions in the close vicinity of the doping sites, something that is proved to increase eventually the electrical resistivity ([5]) ([22].). Even further decrease of the resistivity of the thin film can be achieved with the further addition of Si atoms in the lattice by an accompanied secondary precursor of Si source ([5]).

Based on this literature, we aiming to the systematic polycrystalline SiC growth with low pressure chemical vapor deposition, and study its properties as a possible based material for neural microelectrode fabricated device. As a possible conductive material the films could be suitable for a possible recording or stimulating site of an electronic microelectrode array chip. The physical and chemical properties are originating by the optimal conditions of its deposition, since the deposition conditions determines the stoichiometry, the crystalline and surface quality and the overall conductivity of the thin film. In our approach we investigate the growth of poly-SiC in a low pressure cold-wall system, based on the state-of-art condition ranges that are displayed on Table 1.4.1. The characterization of the deposited films is arranged by various experimental techniques that are described further on (Chapter 2).

Chapter 2: Experimental Methods

2.1. Low Pressure Chemical Vapor Deposition

Low Pressure Chemical Vapor Deposition (LPCVD) is a vapor deposition technique that takes place in the 1-100 mbar of pressure range and 600°C-1300°C temperature range conditions. The reactor can be either hot wall or cold wall with a similar efficiency on the deposition. Either horizontal or vertical reactor configuration can participate in a low pressure procedure with similar results. A common CVD experiment combines many different aspects of science and engineering like thermal physics, chemistry, fluid mechanics and many more. The CVD process corresponds to the reaction of chemical compounds in the vapor phase near the heated substrate to form a high quality solid deposit ([37]). The principal chemical reactions utilized in CVD growth are thermal decomposition, reduction, oxidation and formation reaction. These actions can be used individually or conjunctly. The properties of the deposited thin films are directly affected by the experiment's optimal conditions. The optimal conditions are including but are not limited to the ambient temperature, the hot-zone pressure, the precursor's standard chemistry and flow rate and the growth duration. The details on CVD experiment used in this work are given in Chapter 3. Figure 2.1.1. illustrates the basic mechanism of a possible CVD reaction. The main CVD process is achieved following these physical steps.

1. Inlet of precursors into the reactor, close to the substrate surface.
2. Gas phase reaction close into the hot zone of the reactor.
3. Diffusion of the reactance on the substrate surface.
4. Adsorption of the species on the substrate surface.
5. Diffusion of the adsorbed species into favorable sites.
6. Desorption of bi-products away from the reactor's hot zone.

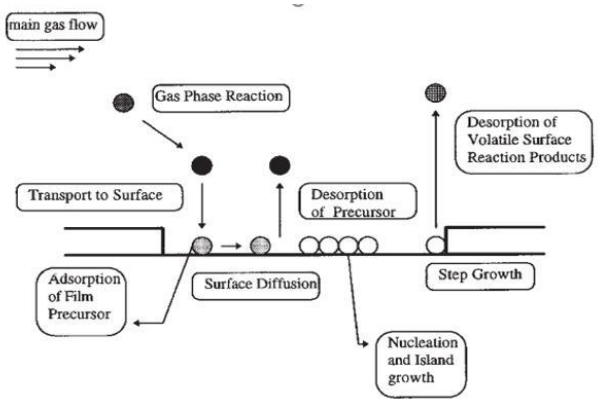

Figure 2.1.1. Precursor transport and reaction process in CVD.

The selected precursors were the silane SiH_4 diluted in hydrogen (3% in H_2) as a silicon Si source and the propane C_3H_8 as the carbon C source. Hydrogen $H_2$with steady flow rate at 390 sccm is used as the carrier gas. The pressure is kept steady during deposition at 20 mbar. The heating is performed by an RF inductor that is oriented around the induction chamber. An exhaust pump system enables the outlet of the gaseous byproducts. A water cooling system around the quartz tube is set on 80^{o}C, throughout the deposition duration.

2.2. Characterization of thin Films

Characterization of deposited thin films can be achieved by various experimental methods according to the studied parameter. Table 2.2.1. displays the experimental method and the corresponding parameter of the deposited thin films they characterize. The experimental methods are described further on the next few contents of this chapter. Each method can illustrate a single or multi parameter evaluation.

Experimental Method	Parameter
Scanning Electron Microscopy	**Layer Thickness (μm)**
X-Ray Diffraction	**Structural quality**
Raman Spectroscopy	**Structural quality**
Optical Profilometry	**Average Surface Roughness (nm)** **Surface curvature (m^{-1})**
Four-point probe measurement	**Electrical resistivity (Ω*cm)**
Cyclic Voltammetry	**Charge Storage Capacity (mC/cm^2)** **Charge Delivery (per phase) (μC)** **Capacitance (μF)**
Electrochemical Impedance Spectroscopy	**Electrochemical Impedance (Ω @ 1KHz)**

2.2.1Scanning Electron Microscopy (SEM)

Scanning Electron Microscopy (SEM)is a microscopy technique that produces images of a sample by scanning the surface with a focused beam of electrons. These electrons interact with the atoms of the sample and the produced signal is providing information about the topography and the composition of the sample ([24]). SEM technique is very common in

the study of thin films. Here, cross section SEM is used for the evaluation of the thickness of the deposited thin film.SEM observation can also be associated with the evaluation of the average surface roughness, although the cross section technique is not a suitable one for this purpose. The roughness can be identified by a profilometry technique either by probe or by irradiation to the surface, that is described in detailed in the next content. Usually for the observation of conductive or semiconductive materials an electron accelerating voltage is ranged between 3kV and 5kV.

2.2.2 Optical Profilometry

Optical Profilometry is a technique that is used to extract topographic data from a surface. This can be a point, a line or a surface or ever a full three dimensional scanning. The main purpose of the profilometry is to gain information about the surface morphology, step heights and surface roughness ([25]) ([26]). The light is sent in a way that can detect the surface in 3D. An optical profiler is a type of microscope in which white light from a lamp is split into two paths by a beam splitter. One path directs the light onto the surface under test, the other path directs the light to a reference mirror. Reflections from the two surface are recombined and projected onto an array detector. When the path difference between the recombined beams is on the order of a few wavelengths of light or less interference can occur. This interference contains information about the surface contours of the test surface. The overall printed result is what is called as surface profile. Mechanical stress of a thin film can also be evaluated through this optical technique. An optical profilometer is usually able to calculate the curvature value of the scanned area. Based on this information and the deposited thickness of the thin film, the residual stress can be successfully estimated. The residual stress σ_c of a thin film can be then calculated using the known Stoney's formula (2.1) ([27]).

$$\sigma_c = \frac{E_s}{1 - v_s}\frac{t_s^2}{t_c}\left(\frac{1}{R_C} - \frac{1}{R_0}\right) (2.1)$$

Where Es is the Young's modulus of the substrate, v_s is the Poisson ratio of the substrate, Rc is the radius of curvature of the thin film and R_0 is the radius of curvature of the substrate. The t_s and t_c values are the thickness of the substrate and the thin film respectively.When the σ_c value is positive then the film is tensile, while a negative calculated value, ignites that the film is compressive stressed. The optical measurement does not affect the measured stress of the film and the overall experimental technique is a non-destructive one.

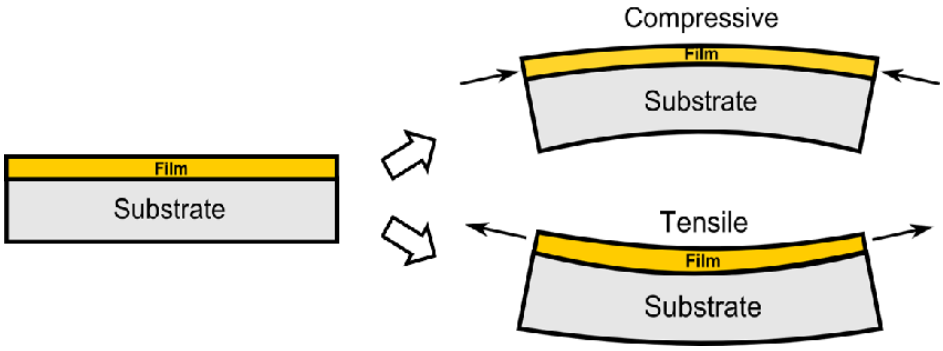

Figure 2.2.1 (Left) Deposited thin film over the substrate layer configuration. (Right-Up) Compressive configuration of the deposited thin film on top of the substrate. (Right-Down) Tensile configuration of the deposited thin film on top of the substrate ([27]).

2.2.3 Four-point probe Electrical Resistivity

The four-point probe electrical resistivity is an experimental technique that is used to measure the electrical sheet resistivity of semiconducting films. Two individual probes are introducing steady electric current to the thin film surface, while two secondary probes are measuring the voltage drop between the two initial terminals. Sheet resistance (or surface resistance) is a common electrical property that is used to characterize thin films of semiconducting materials ([28]). Technically is the lateral resistance between the two opposite terminals of a square piece (or rectangular piece in general) of a semiconducting thin film. The probes must be oriented in parallel during the experimental process. Figure 2.2.2 illustrates the experimental set up of sheet resistance measurement. The sheet resistance can be calculated using the equation 2.2. Then the resistivity for thin films up to 20μm can be calculated by just multiple the sheet resistance R with the thickness of the thin film d, shown by the equation 2.3. Besides the sheet resistance, parasitic resistances can be occurred, responsible of failing to acquire the precise sheet resistivity of the film. Usually the resistance components are the common wire resistance R_w and the contact resistance R_c, which is occurred during the direct contact between the probe and the thin film. Usually a high conductive material is used as probe, in order to minimize as possible the contact resistance in the interface.

A Signatone instrument is used equipped with a tungsten carbide (WC) 4-probe head, for the acquisition of the sheet resistivity. Signatone is supported by a Keithley current generator that delivers the current input. The generator is set to deliver current of 60mA maximum, while the voltage recording range is specified between 0 to 100mV for both positive and negative current input. The bipolarity is useful while studying non isotropic and rough surfaces. Since each crystalline direction it's not directly identical to its relatives, it can exhibit significant difference in the responded sheet resistance. Thus by bipolarity every possible direction is tested, gaining the average sheet resistance of the studied film.

$$R = 4.53236\frac{V}{I} \quad (2.2)$$

$$\rho = R*d \quad (2.3)$$

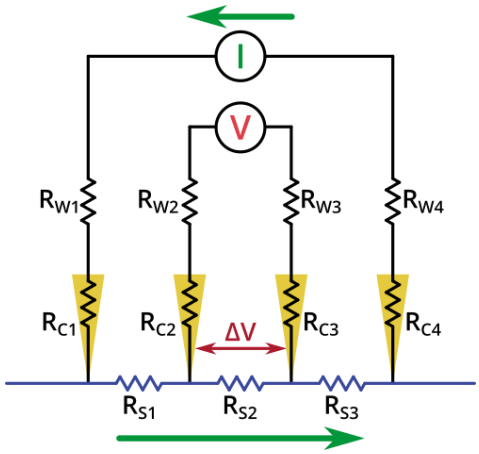

Figure 2.2.2. Four Terminal Electrical Resistivity set up. The steady electric current is passing through the two outer probes, while the measured voltage drop is directly measured within the two inner probes ([28]). The parasitic resistances are caused by the common wire resistance, Rw and the interface-contact resistance Rc. Usually these two resistances are many orders smaller than the measured one Rs, such as they don't interfere and lead to a false measurement.

2.2.4 Cyclic Voltammetry

Cyclic Voltammetry (CV) is among others an important experimental technique for electrochemical measurements and the characterization of electrodes. This technique makes use of the electrochemical cell. The cell is the primary experimental set up, that can either produce or expense electrical energy via or for the process of an appropriate chemical reaction ([29]). The cell is containing the working electrode (WE) and the counter electrode (CE), through which the current is passing and the reference electrode (RE), in reference of which, the input potential of the WE is measured. It is needed to notice that the potential itself of the RE remains steady throughout the cyclic voltammetry process. The potential difference (voltage) input is applied between the WE and the CE, but it is ultimately measured between the WE and RE terminals.

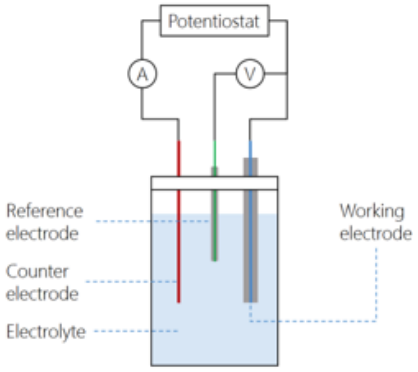

Figure 2.2.3 The electrochemical cell. The potential is recorded between the Working electrode (Blue) and the reference electrode (Green), while the current is recorded between the working and the counter electrode (Red).

In cyclic voltammetry the voltage is swept linearly until the desired voltage limit, and then sweeps linearly the opposite direction until the initial starting point. For example a used voltage range for neural stimulation is the (-0.7V, +0.7V), while for electrochemical battery reasons the range (-1.4V, +1.4V) it is widely used. In this way it is performed a circle of voltage scanning inside the cell. Electrochemical phenomena occur in the first-half as well as in the second-half of the linear voltage sweep. The resulted graph is the common voltammogram with a "duck shape" curve ([30]). The duck shape diagram result is common for a redox chemical reaction during the procedure. Half of the duck shape diagram (from 0 to C, Figure 2.2.4) is referring to an oxidation inside the electrochemical cell, while the other half (from C to 0 Figure 2.2.4) indicates the reduction of the system. Whenever a chemical redox reaction takes place, charge transfer is occurred, resulting to a current response, which is called Faradaic current. While the charge transfer rate remains steady the Faradaic current acquires linear profile. Figure 2.2.4 displays the Faradaic current response, for either oxidation (from A to B) or reduction (from D to E) reaction. Faradaic current can only occur in a redox species cell. In another case there can be no charge transfer during the voltage sweep and no oxidation or reduction can happened on the WE surface.

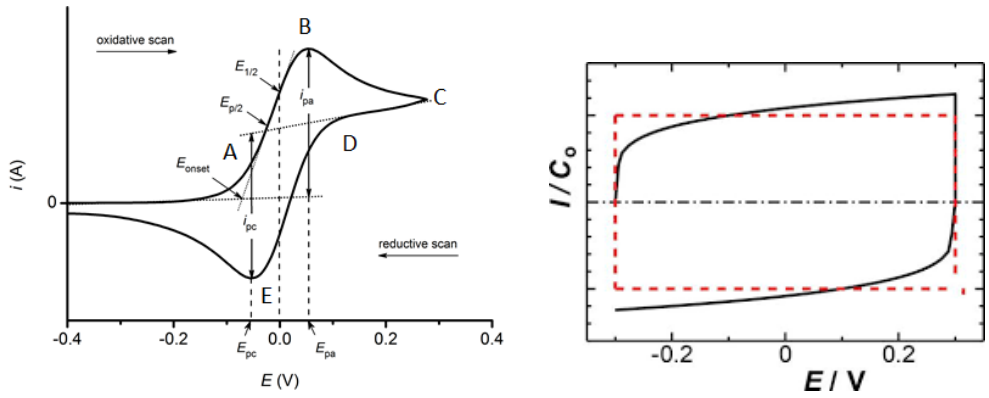

Figure 2.2.4(Left) The common ideal cyclic voltammogram of "duck-shaped" curve, with chemical redox species. Potential values of E_{pa}(anode) and E_{pc} (cathode)i_{pa} (anode) and i_{pc} (cathode) are indicating the peak values of current. (Right) Capacitive current response I vs. E diagram. Red line indicates the ideal theoretical response while the black one shows a compatible response ([29]), ([30]).

When the electrochemical cell does not contain redox species, it can still deliver electric current through the WE by the formation of the electric double layer of Helmholtz. This happen in buffer solution which are solutions with steady pH that cannot participate easily to a redox process. In this case the surface of the WE and the electric double layer form the two terminals of an electrical capacitor with the solvent to be the dielectric between the two terminals. The corresponding current output through the WE surface is called capacitive (Figure 2.2.4 right). In general, the pure capacitive response displays an RC circuit behavior, having an initial charge until it reaches a constant value that holds until the end of the voltage sweep ([35]). The double layer capacitance per unit surface can be acquired by dividing the background current density with the applied scan rate ([9]). Background current is the value of current whenever the potential difference between WE and RE is zero (V=0). Both background currents for anode and cathode can defined with the same way. It is very usual also for the case of electrochemical capacitors to demonstrate the average capacitance of the

electrode. According to the mathematical definition of pure capacitance, the corresponding capacitive current acquires linear profile according to the scan rate, assuming that the average capacitance is steady.

$$I = C\frac{dV}{dt} \text{ (2.4)}$$

Cyclic Voltammetry has been proved very useful when evaluating electrochemically, an electrode device for neural interface applications. Many *in-vitro* studies suggest that the evaluation is performed in terms of capacitive behavior inside PBS buffer solution. This solution demonstrates the most accurate behavior comparing to the real isotonic ambience round the neural tissue of the brain. It has become a common practice to estimate the charge storage capacity (CSC), for both anode and cathode process, which is an estimation of the total amount of the charge that an electrode has available for a stimulating pulse, in a slow sweep rate ([31]). The CSC can be estimated by the average capacitance C multiplied by the scan rangeΔV. Along with CSC, it is also common to estimate the charge deliver (CD) for either anode or cathode phase, which is the overall charge that it is transferred from and into the electrode throughout the potential scan range, for either anode or cathode process. Mathematically it can be defined as the background current over the scan rate, v multiplied by the overall scan range ΔV.

$$CSC = \frac{C*\Delta V}{A} \text{ (2.5)}$$

$$CD = \frac{I}{v} * \Delta V \text{(2.6)}$$

Charge storage capacity is usually more desirable than the faradaic current response because no chemical species are created or consumed, via a chemical reaction, during a stimulation pulse. Faradaic electrodes like Pt and other metals can provide high levels of charge injection during stimulation. However, changes in the electrolyte composition adjacent to the electrode and the finite rate of faradaic reactions can lead to irreversible processes that can cause electrode or tissue damage ([8]).

2.2.5 Electrochemical Impedance Spectroscopy

Electrochemical Impedance Spectroscopy (EIS) is known to the electrochemistry community as an active characterization technique of the electrochemical impedance of active electrodes. Impedance is a measure of the overall resistance a circuit experiences related to the passage of an alternative current (AC). In an AC system, the applied signal is not static like the direct current system (DC) but oscillates as a sinusoidal wave at a given frequency. The expression of impedance is analogous to the Ohm's law for the static resistance.

$$Z = \frac{V(\omega)}{I(\omega)} \quad (2.7)$$

The impedance of an electrochemical system is measured by applying a small AC potential and then measuring the resulting current through the electrochemical cell. Normally EIS measurements are using a wide frequency range scan [0.1Hz – 1MHz]. The measurements employ small sinusoidal excitation signals, where the root means square (RMS) magnitude of the excitation source is usually kept at approximately 5-10 mV ([32]). The current response will be also a sinusoidal wave function, with the same frequency, but with a phase shift. The three electrode configuration allows for the measurement of potential frequency sweeps of the WE independent of changes which may occur at the counter electrode. For in-vitro studies the electrolytic solution in the case of neural equivalent environment is the phosphate buffered saline (PBS). Electrochemical impedance can provide useful data on electrode impedance and capacitance. The real impedance of an electrode is the direct result of its resistance R, capacitance C and its inductance L. Normally, in a usual electrochemical system the electrolyte's resistance, slow electrode kinetics, slow chemical reactions, double-layer capacitance and diffusion can all impede the flow of the current and therefore, are analogous to the impedance elements of an AC circuit.

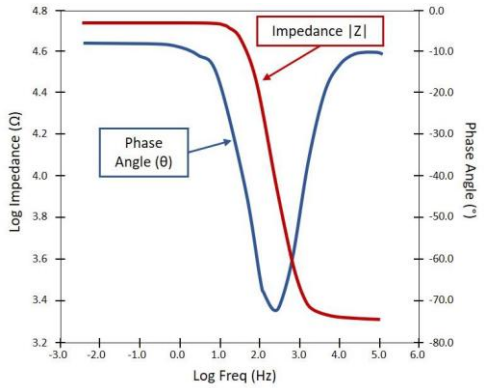

Figure #.#.#. A generic Bode plot of electrochemical impedance Z. Red curve represents the log plotted impedance Z against the log frequency and the blue one presents the phase angle vs. log frequency as well. By utilizing both graphs, various circuit elements (R, C, L) of the electrochemical cell can be extrapolated to model the electrode equivalent circuit and its overall performance ([32]).

EIS measurements are often displayed on a Bode and a Nyquist plot. In the case of the electrode impedance the Bode plot gives directly information about the overall impedance of the electrochemically active electrode, regarding the frequency evolution. The Bode graph provides two specific plots. The first plot is a plot of the overall impedance magnitude (Z) according to the frequency of the applied AC potential and the second one presents the Phase angle as a function of the same frequency range.

2.2.6 Raman Spectroscopy

Raman Spectroscopy is an analytical technique where scattered light is used to measure the vibrational energy modes of the sample. It can provide both chemical and structural information, as well as the identification of substrates through their characteristics

Raman fingerprint. ([33]). In the classical theory, each active Raman vibration mode is a result in the change of the polarizability of the molecule during its interaction with the incident photon ([33]), ([34]). In the quantum theory each vibration mode obeys a specific selection rule of excitation, according to the type of the excitation and the freedom degrees of the molecule's motion.

A Renishaw Raman Spectrometer analyzes the back scattered Raman radiation of the sample, which is caused by the excitation of a 512 nm green laser. Although that the exposure time can be varied, it remains overall steady at 20 sec for a fast scan, holding high quality recorded signal. The laser power is steady at 10mW. The spectrometer is recording only the Stokes scattering range, as the Anti-Stokes scattering remains pretty weak in intensity to be considered important.

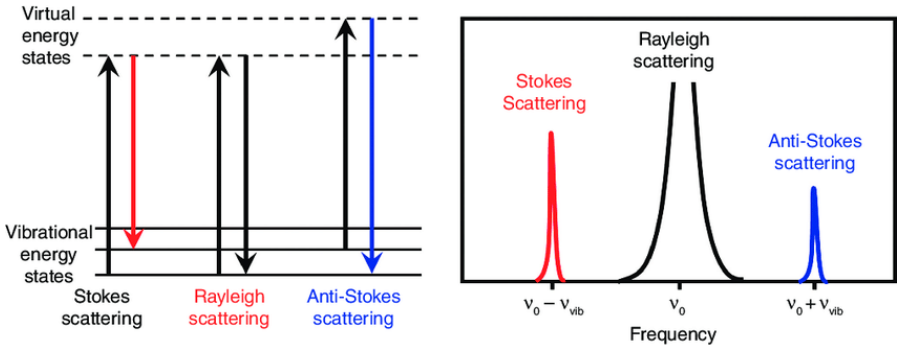

Figure 2.2.5. Jablonski diagram for Rayleigh and Raman scattering ([34]).

2.2.7 X-Ray diffraction

X-ray diffraction (XRD) is an important characterization tool to study crystallographic properties of the epitaxial layers. In fact, the wavelength of X-ray and the typical inter-atomic distance in crystalline solids are on the same order (a few angstroms, 1Å = 0.1nm), which makes X-rays the correct order of magnitude for diffraction of atoms of crystalline materials. XRD can provide structural information such as lattice constants, orientation, strain and dislocation density in the layer.

The experimental set-up of a diffractometer consists of an X-ray source equipped with a monochromator, and a gas ionization detector, and the sample is analyzed, explaining the interference of X-rays from lattice planes, by the following equation:

$$n\lambda=2d_{hkl}\sin(\theta) \quad (2.8)$$

whereλ the wavelength of x-rays, d_{hkl} the lattice plane spacing, n the order of the reflection and 2θ the angle between incident and reflected X-ray.

Two basic types of scans, namely, ω scan and ω-2θ scan, are usually used for structural characterizations to provide information about crystal quality of the measured material. ω is the angle between incident X-ray and sample surface whereas 2θ represents the detector angle. In the ω rocking curve measurement, the 2θ is fixed to the position $2\theta_0$of the Bragg peak. In this case, only one lattice plane spacing will be studied. ω is tilted around the Bragg peak. ω scan is sensitive to strain, dislocations and mosaic structure in thin films.

Chapter 3. Polycrystalline SiC growth

The deposition of Poly-SiC is described in the present chapter. A major part deals with the optimization method employed to reduce the number of the growth experiments. Towards this purpose many experimental results from the physical characterization of the samples are mentioned n the present chapter although the analytical results are included in the following chapter 4.

3.1 LPCVD deposition of polycrystalline SiC thin films

The deposition was completed using quartz, vertical, cold-wall reactor. Figure 3.1.1 presents the schematic of the vertical CVD system. Various experiments were performed in order to find the optimal conditions for the simple deposition of an undoped polycrystalline SiC thin film, before proceeding with the n-doped polycrystalline SiC deposition.

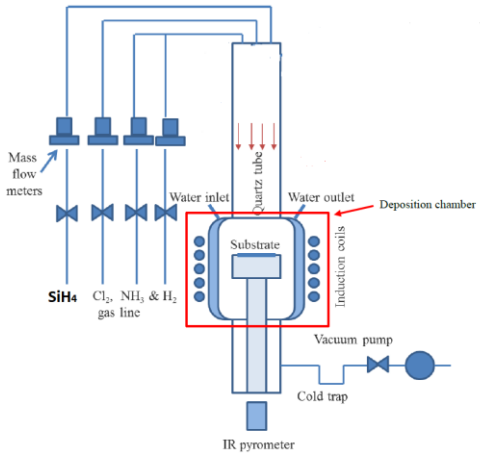

Figure 3.1.1. Vertical cold wall LPCVD reactor schematic. The red square indicates the deposition chamber. The susceptor is placed in the middle of the chamber where the substrate is oriented on it. Gas flow is distributed from the top of the reactor (red arrows). As a cold-wall reactor the hot zone is the chamber itself.

The experimental procedure is described by the following steps:

1. Three-times purging with argon Ar gas.
2. Pressure is set on 20 mbar and H_2 flow at 390 sccm.
3. Thermal annealing to growth temperature and 5 minutes stand-by.
4. Gases inlet to reactor for deposition.
5. After deposition, the system is cooled down to room temperature.

6. Three-times purging with argon Ar gas.

3.2 Preliminary growth experiments

Preliminary growth experiments were used to evaluate general growth conditions. Polycrystalline SiC thin films were deposited on epitaxial Si (100) wafers. The deposited thickness was found to be around 8μm on average, using the cross section SEM technique. The films were grown between 900^{o}C and 1100^{o}C ambient temperature. The flow rate of silane and propane are respectively set to 7.5 sccm and 5 sccm giving a chemical gas phase ratio value of C/Si:2. The thickness was found varying within the same thin film, indicating a non-uniform deposition. The non-uniformity is resulting by the orientation of the wafers on the susceptor. It is possible the biggest thickness to be resulted in the wafer's sites that were exposed to the center of the susceptor, while the least exposed sites were having less but steady growth of thickness ([37]). This fact should be a reasonable result of a possible inhomogenity of temperature (as long as our reactor is in the kinetic limited regime) or a possible speed gradient (as long as the reactor is in the mass transport limited regime). Table 3.2.1. displays the results of the first calibration experiments. The films are evaluated in terms of layer thickness, average surface roughness and sheet resistivity.

Dichloride gas has been also introduced in the reactor as an accompanied gas. The experimental results of the Table 3.2.1 show that the deposited thickness is significant lower under chloride treatment. Such results suggest that chloride indeed performs strong etching during the deposition. Chloride treatment has also a big effect to the corresponding electrical resistivity.

The chloride treated films result into significant lower sheet resistivity compare to the ones that didn't growth under chloride ambience. The resistivity value is decreased almost three orders, suggesting that a specific surface mechanism under chloride ambience lowers the overall resistivity. Several hypothesis could explain this behavior: Scattering sties from rougher surfaces, modification of grains size and the corresponding number of grain boundaries. ([38]). The mechanism discussed in detail later (Chapter 4.2).

First test of in-situ doping has been performed in 900^{o}C ambience temperature, while keeping the Cl/Si value steady. The gas phase ratio value of N/Si was set approximately to 0.25. Electrical resistivity measurements show that with *in-situ* doping resistivity as low as 0.02 Ω*cm can be achieved. The resulted thickness is similar with the previous experiments on chloride ambience, confirming once again the possible etching mechanism provided by the chloride gas. On top of that the average surface roughness is increased with the introduction of nitrogen, something that agrees with previous doping studies ([5]). The increase in the surface roughness might be caused by the impeded nitrogen atoms inside the lattice, as it was mentioned before (Chapter 1.4).

The increase in the flow rate of silane showed no significant increase on the deposited thickness. Since only the growth duration has been changed, while all the growth parameters remain steady, it could be descent to consider that our rector is on the kinetic limited regime of operation. This fact could explain also the fact of the non-uniformity of the deposited thickness, between the center and the sides of the substrate, as mentioned before. Since the

chemical decomposition of the precursors is deeply affected by the growth temperature, a thicker layer of SiC is expected to grow, on the highly thermal exposed center of the substrate's surface.

Name	SiH_4 3% in H_2 (sccm)	C_3H_8 (sccm)	Temp (°C)	C/Si	Cl/Si	N/Si	Duration (min)	Thickness (μm)	RMS (nm)	ρ (Ω*cm)
MG-SiC-01	250	5	1100	2	0	0	30	6.5	80	102.31
MG-SiC-02	250	5	900	2	0	0	30	9	60	6000
MG-SiC-03	250	5	900	2	0	0	60	7	21	6200
MG-SiC-04	250	5	900	2	2	0	60	0.5	7	4.61
MG-SiC-05	250	5	900	2	2	0	150	0.4	9	11.80
MG-SiC-06	500	10	900	2	2	0.25	90	1.2	34	0.015

Table 3.2.1 List of the experiments for the calibration of the used reactor.

3.3 Design of experiment (DOE) for n-doped poly 3C-SiC thin film deposition

After preliminary growth test, the DOE methodology has been applied to the LPCVD process and as a next set of experiments, which is discussed as follows. For the best quality and systematic study of the experimental results we are willing to use a Design of Experiment (DOE) technique especially for the low pressure CVD deposition. With the DOE tool we gain significant information about the optimal condition system with the lowest amount of required experiments. Since the CVD experiments tend to be expensive enough, with the DOE we minimize directly, as much as possible, the expenses in terms of resources and available materials, providing high quality results in the investigated experimental approach.

Design of experiment (DOE) technique is an experimental design method that is widely known in the industrial research domain for the high quality and accurately experimental settings determination and technology development ([39]). When it comes to CVD-deposition-of-thin-films experimental design, it is very important to set the best possible input parameters (growth parameters), determining the output values (targeted physical properties). The chosen input parameters are varied linear, from a low to a high value, according to their possible effect on the output values. The values of the input parameters are marked as -1, 0 and +1, with -1 indicating the low value; 0 indicates the central value and +1 indicates the high value. There is no limitation on how many inputs and output parameters could be chosen for a DOE. The main purpose of this technique is not only to unveil the best optimal parameters but also to study the fundamental effect of the chosen inputs to the desired outputs.

It is common practice in the CVD studies to follow the Hadamard matrix DOE technique ([39]). This method suggests that the experimental studies should begin by a really confined central point of input parameters and check very quickly the reproducibility of similar results in three consecutive experiments. The latter are called the central point experiments. When the reproducibility is confirmed the DOE is continued following the Hadamard matrix configuration by varying the input parameters (an example is the data of following table 3.4.3). Following, a fourth central point experiment is conducted to confirm

the reproducibility and the reliability of the input variables. The final experiment is called «-1» experiment, since only the «-1» experimental inputs are allowed. This experiment tends to show the aspects outside of the main experimental boundaries.

Typical graph is resulting from the doe analysis is shown in figure 3.4.2. For each output the possible influence of input is evaluated. The mean value and standard deviation among all the central points (same experiment) is evaluated. Then when the bar is above or below 2 sigma, it indicates a statistical influence of the parameters. The effect of the input parameter is valid only when the corresponding variation is bigger than the double amount of the standard deviation of the measured output parameter (2σ). There are cases that the variation passes the triple amount of standard deviation (3σ), indicating the dominating effect of the input to the measured output parameter.

Additionally with the histogram, an order graph illustrates the progress of the measured output value of a chosen parameter, with respect to the order of the performed experiments ("order of experiments"). Completing an order graph, it is possible to observe whether a value of a measured parameter is drifting or not. In the first three central point experiments it is very important, the value of the parameter to not show significant drifting, as this indication is recommending a non reproducible output in the same optimal conditions. In such conditions the DOE cannot be performed efficiently and thus it is recommended to set a new central point values, as long as the ultimate goal is the control of the output value of the measured parameter.

Input parameter	Values of Input parameters		
	-1	0	+1
Temperature	900^{o}C	1000^{o}C	1100^{o}C
Cl/Si	0	1	2
N/Si	0.05	0.15	0.25

Table 3.3.1.DOE-technique-input parameters and their specific values for the LPCVD growth of poly SiC

It is worth to mention that the three input parameters are chosen according to the maximum effect they present in the deposition of polycrystalline SiC thin films, based on the state of art itself and from previous scientific experience. The temperature range is varied between 900^{o}C and 1100^{o}C. Studies have shown that this range is capable for polycrystalline SiC growth with a similar standard chemistry like in our approach ([5]). The Cl/Si ratio value shows the amount of the induced chloride species into the reactor. It can vary numerically between 0 and 2. It has been shown that in such gas ratio values, chloride can significantly preventing the growth of polycrystalline Si during the deposition, enhancing such the quality of the grown SiC ([23]) ([48]). It has been also reported that it can probably participate to the

control of the film's residual stress ([5]). The gas ratio N/Si is determining the doping efficiency of the thin film. It has been reported that nitrogen atoms can participate as successful donors since their atomic electronic structure contain one excess electron than of Si and C themselves. Each nitrogen atom can be ionized easily, by providing an excess free electron to the conduction band of the SiC, enhancing the film's conductivity behavior. Although most of the studies stop at N/Si:0.05 value, in our approach we extent this study beyond that value, investigating the effect of heavy doping to the conductive behavior and the crystallinity of the n-poly-SiC.

Physical and chemical conditions have also been determined as fixed parameters during the DOE technique. These parameters usually have no influence on the deposited thin film. In our approach the fixed parameters are consisting of the C/Si ratio, the ambience pressure, the precursors flow rate and the duration of the deposition. The C/Si value is remaining steady at 2, targeting to a non-silicon rich thin film, as silicon rich SiC films have shown multiple crack-sites. The ambience temperature is set at 20mbar steady, as this is consisting an automated parameter of the used, custom made reactor. The flow rate of diluted silane is set at 500 sccm. The choice of the bigger flow rate is related with a possible increased growth rate, as it has been shown in previous studies of poly-SiC. The deposition duration is set at 90 minutes. In many cases of poly-SiC the deposition ratio is varied between 60-120 minutes ([7]) ([21]) ([22].).

The output parameter are determined from previous studies of n-doped poly SiC studies for neural interfaces and MEMS applications showing their importance for the final application.

	Investigated output parameters
	Layer Thickness
	Root Mean Square of surface roughness
	Residual Stress
	Sheet Resistivity
	Charge Storage Capacity
	Charge Delivery per phase
	Capacitance

Table 3.3.2. List of the investigated output parameters for the DOE polycrystalline SiC deposition.

Table 3.3.2 displays the output parameters of our DOE study. Based on this table the analysis of DOE is presenting the effect of each input parameter to the output parameter. In the following subchapter the specific histograms are presented with the same order of the output parameter, as displayed in the 3.3.2 table.

3.4 Results of poly-SiC growth optimization study following DOE

Figure 3.4.2 presents the histogram and the order graph of the deposited average thickness. The histogram shows that the Cl/Si ratio has the biggest statistical influence on the average thickness, exceeding the -2σ value and shows an inverse relationship between them. Meaning that an increasing value of Cl/Si, is resulting in a decreased deposited thickness. The more induced chloride into the reactor the thinner the deposited film. The reduced thickness

could suggest that the induced chloride might perform a strong etching during the deposition process in the growing film. This etching process is taking part during the deposition scratching small flakes of the growing film. Thus a thinner film is deposited.

Ambient temperature has a weaker effect on the average thickness, holding a proportional relationship with it. The increased ambient temperature enables the decomposition of larger amount of the precursors, due to the higher kinetics between them. Thus the more frequent and efficient chemical reaction is occurred close to the substrate surface, the more available active species are present for adsorption in the inner surface of the substrate. The surface diffusion is also thermally enhanced in the temperature elevation. Thus the growth rate is increased along with the corresponding thickness.

The N/Si has no relevant effect on the average thickness, holding an inverse relationship between them. It is shown that the induced nitrogen tend to decrease the average thickness. This could suggest that the amorphization on the doping sites and the reduced crystallinity is associated with the reduction of the thickness. As the temperature, this parameter value is below the 2σ value, responding to a weak effect on the eventual thickness of the deposited film.

The order graph shows an almost steady value of the average thickness in the experimental progress, with no significant drift of the observed value except two cases. The one shows that in the absence of chloride, during deposition the grown thin film tends to be thicker, while reaching up to 20μm. The second one shows a 3μm thin film, deposited in an intense chloride ambience growth conditions. The low thickness is probably associated with an intense etching that performed by the chloride flow rate. This confirms the effect of the induced chloride, during deposition.

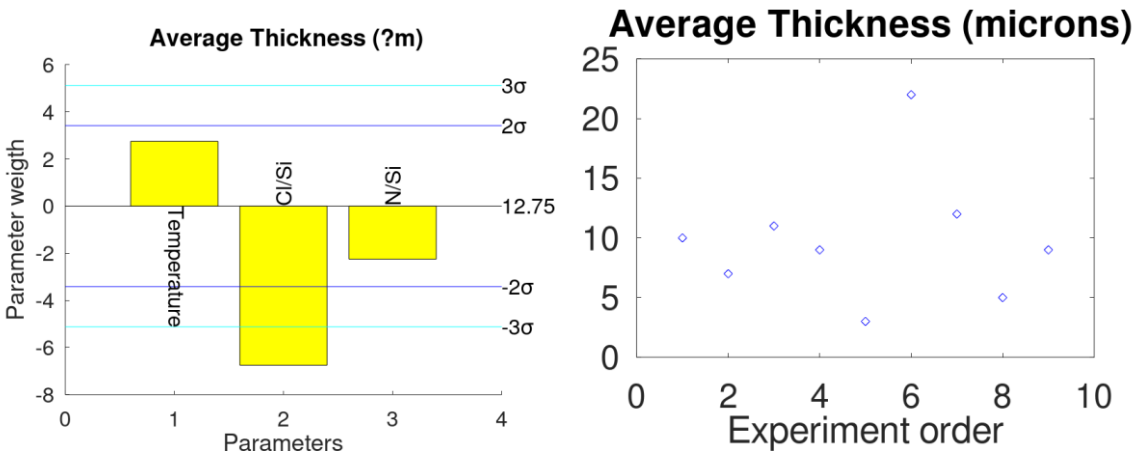

Figure 3.4.2. (Left) Effect of the growth parameters in the average thickness of DOE thin films. (Right) Order graph of the average thickness of the DOE thin films.

The average surface roughness is estimated by the root mean square (RMS) value. The histogram on Figure 3.4.3.presents the parameter weight of the growth conditions on the average surface roughness. Once again the ratio Cl/Si has the biggest effect on the surface roughness, staying above the -2σ value, with an inverse relationship. The induced chloride tends to strongly modify the surface quality, reducing significantly its roughness.

Temperature is the second most important parameter, on the modulated roughness, exhibiting an inverse relationship this time. But once again, the effect is pretty small, as long

it doesn't approach the -2σ. Normally the elevation of temperature is resulting to rougher surface, since the average grains size is also increased. In our case we don't observe such behavior that might be directly related with the averaged grains size, which remains almost steady in this region of temperature, along with the induced chloride.

The ratio N/Si is the weakest parameter of this approach, with no effect on the surface roughness. The relationship between the N/Si and surface roughness is inverse, something that is opposite to previous poly-SiC doping studies ([5]); although the effect of induced nitrogen in our approach is negligible.

The surface RMS value shows no significant drift, according to the order graph of the surface roughness. Only two experiments show a significant deviation from the first ones, which they lack of induced chloride. This confirms the property of chloride to provide a smooth surface. This results also agrees with the previous calibration experiment results for the un-doped films.

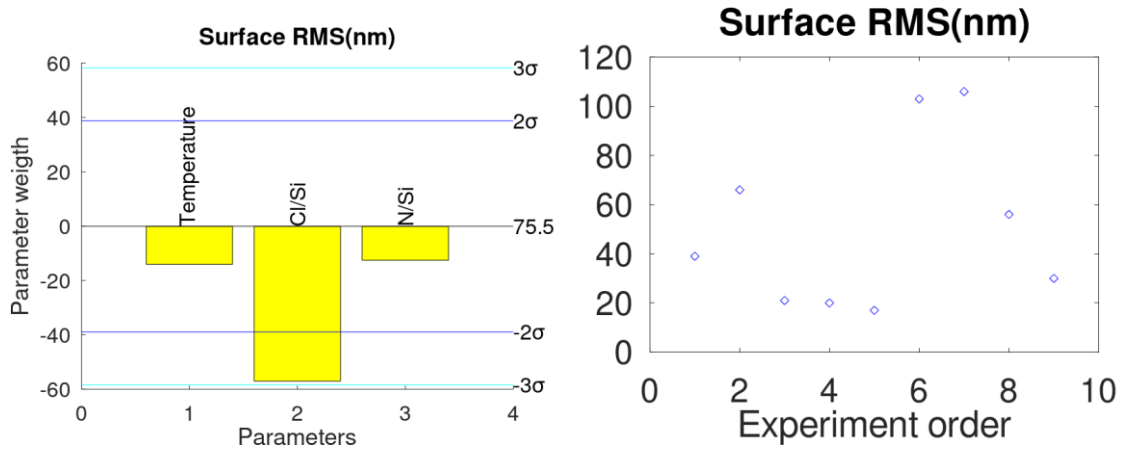

Figure 3.4.3. (Left) Histogram of the root mean square (RMS) of the surface roughness, regarding the deposition's optimal conditions. (Right) Order graph of the surface RMS value of the DOE thin films.

Residual stress is also estimated for all the samples of the DOE thin films. Stress shows to be affected by every growth parameter of the DOE. Every parameter is passing the 2σ value (Figure 3.4.4). Temperature dominates in the stress modulation, while the N/Si ratio follows as the second most affecting parameter. Both of them show to have an inverse effect on the residual stress. The increased thickness, due to the elevation of the temperature, is resulting to lower residual stress. Induced nitrogen seems to decrease the residual stress, something that is opposite to other studies that support that the induced nitrogen tends to increase the residual stress, while using different standard chemistry.

Induced chloride has also a significant effect, although is the weakest of the optimal conditions. The reduced average thickness due to the chloride etching is resulting to an increased residual stress.

The residual stress shows great reproducibility in the first 4 experiments, showing no drift on the order of the experiments. Two of them show significant deviation, and both of them are associated with the chloride amount and temperature.

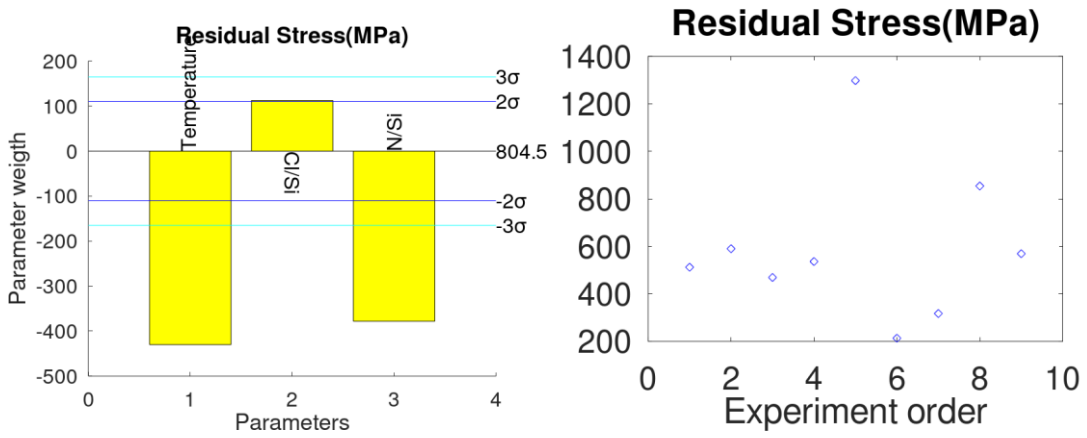

Figure 3.4.4. (Left) Histogram of the effect of the residual stress, regarding to the optimal parameters of DOE. (Right) Order graph for the residual stress of the thin films of DOE.

The histogram of the Figure 3.4.5 shows that chloride is the parameter with the biggest weight of effect in the output resistivity. The ratio Cl/Si value is exceeding by far the -2σ value, while also passes the -3σ value, having also a negative relationship with resistivity. In these optimal conditions chloride seems to have the biggest effect in the output sheet resistivity. Since low sheet resistivity corresponds to very smooth surfaces, it is certain that chloride treatment can have a significant effect on the desired electrical behavior of the surface itself. A decrease in the overall resistivity has also been observed in previous studies of chloride based CVD procedure, although the origin of the chloride effect on the corresponding resistivity, is not yet clear ([5]).

There is no effect of the ratio N/Si. The ratio is showing a negative relationship with the corresponding resistivity. This tension could be explained by the amorphization that is occurred, due to the induction of the nitrogen species into the lattice SiC lattice. The higher amount of nitrogen leads to an increase in the overall resistivity of the thin film. The origin of this increase is not understood yet and not observed in the literature. It could come from the presence of SiNx with too much N content that could modify the resistivity The reason we don't observe a significant effect is probably resulted by the fact that the semiconductor has reached its physical limit of doping.

Ambient temperature doesn't affect the resistivity. It has been shown that deposition temperature may have a significant impact on the corresponding resistivity. The elevation of temperature can result in larger grain size that decreases the sheet resistivity. However in our case we observe the opposite behavior. This may be a result of collaboration between the ambient temperature and the induced nitrogen. In higher temperatures the amount of desorpted nitrogen into the substrate's surface is bigger, due to the easier decomposition of ammonia. The higher amount of nitrogen increases slightly the resistivity due to the extensive amorphization around the nitrogen sites, into the lattice.

The order graph doesn't show significant drift of the resistivity value. The two deviated values are highly associated with the amount of the induced chloride, thus confirming the effect of the induced chloride to the corresponding sheet resistivity.

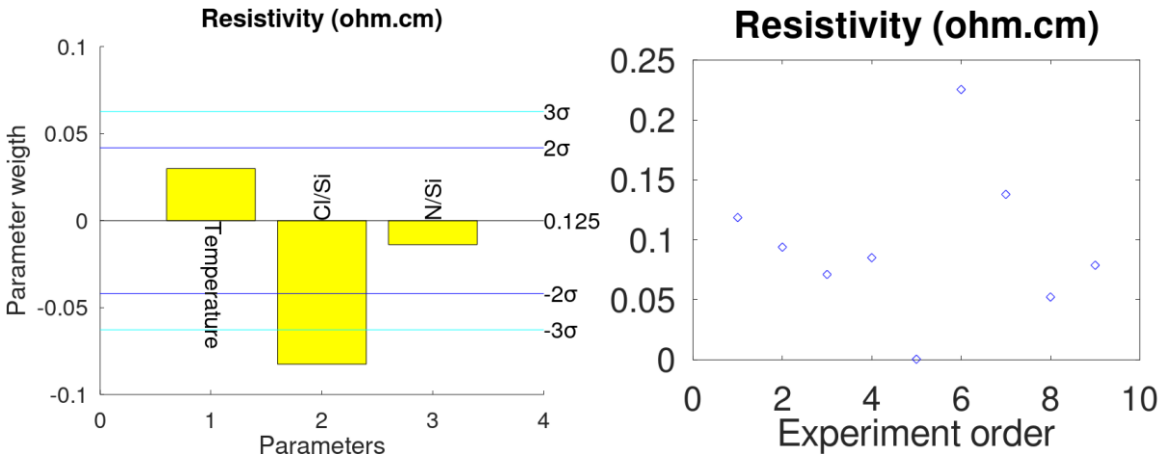

Figure 3.4.5. (Left) Histogram for the effect of the resistivity, regarding to the optimal conditions of DOE. (Right) Order graph of the resistivity of the DOE thin films.

Figure 3.4.6. displays the DOE results of the three electrochemical outputs, by histogram and their order graph. Despite the parameters can have a proportional or an inverse weight between the electrochemical results, none of them is showing a significant influence for any electrochemical output value. The order graphs don't show significant drift between the experimental measured values, despite some negligible cases. But since there is no influence of the input parameters, these cases cannot support a descent explanation on this small drift.

The incapability of the input parameters to influence the electrochemical response of the fabricated electrodes is indicating that the electrochemical response should be associated with the intrinsic characteristics of the deposited film. Since the electrochemical performance is determined by the capacitive characteristics of the film, objects like the electrochemical active area and the amount of the available carriers in the surface of the electrode facing the electrolyte, are the most promising of giving specific information about the electrochemical performance of the electrode. The average grain size, the crystallinity and the average surface roughness combined with the doping efficiency (population of the conductive carriers-electrons), are the main intrinsic features that should be related with the average electrochemical response of the electrode. In Chapter 4. we explain in detail the electrode's features, which they contribute to a typical capacitive response in an electrochemical environment.

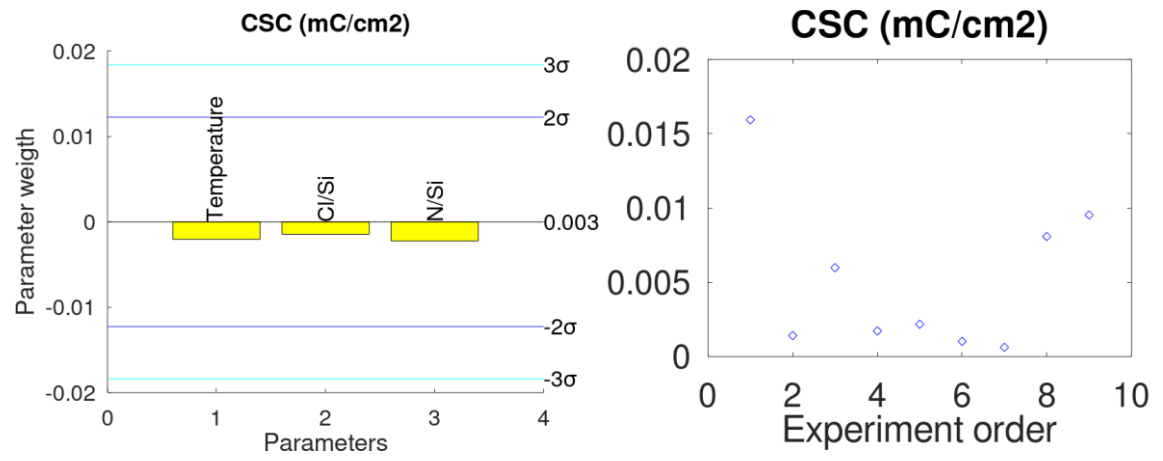

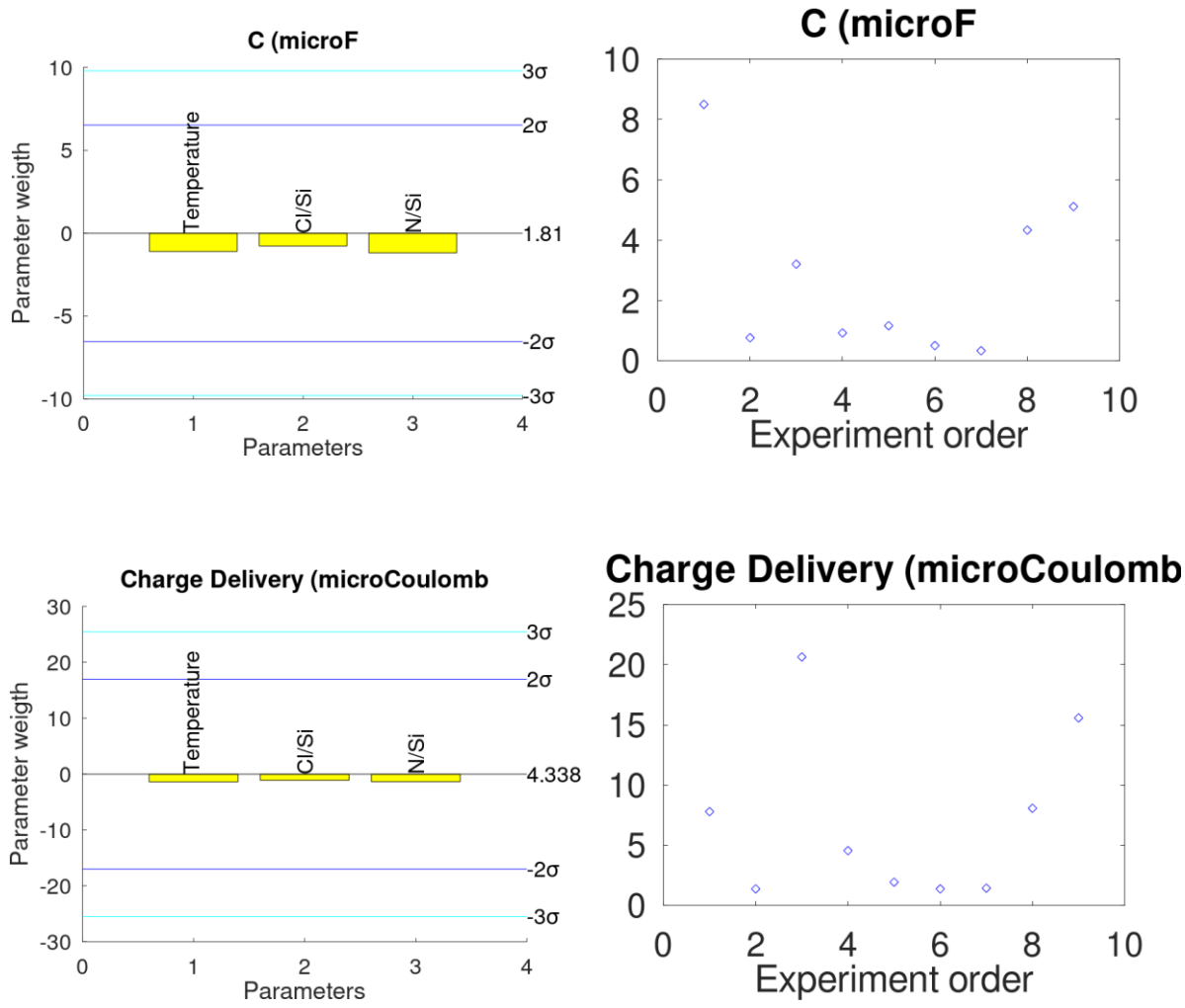

Figure 3.4.6. Electrochemical results of DOE experiments. (Left) Histograms of Parameters and their influence on the electrochemical outputs. (Right) Order graphs of Parameters on the electrochemical results.

Name	Temp (°C)	Cl/Si	N/Si	Average Thickness (µm) ±1µm	Surface RMS (nm) ±nm	Residual Stress (MPa) ±20MPa	CSC (mC/cm^2)	C (µF) ±µF	Charge Delivery (µC)	ρ (Ω cm) ±0.001 Ω*cm
MG-SiC-07 C1	1000	1	0.15	10	39± 1	512	$15.94*10^{-3}$	8.50 ±0.10	7.79	0.1187
MG-SiC-08 C2	1000	1	0.15	7	66± 2	590	$1.41*10^{-3}$	0.76 ±0.13	1.37	0.0940
MG-SiC-09 C3	1000	1	0.15	11	21± 1	469	$5.98*10^{-3}$	3.20 ±2.02	20.64	0.0712
MG-SiC-13 H1	1100	2	0.25	9	20± 9	536	$1.72*10^{-3}$	0.92 ±0.02	4.55	0.0852
MG-SiC-15 H2	900	2	0.05	3	17± 4	1298	$2.17*10^{-3}$	1.16 ±0.16	1.93	0.0005
MG-SiC-14 H3	1100	0	0.05	22	103±25	213	$1.02*10^{-3}$	0.50 ±0.03	1.37	0.2255
MG-SiC-12 H4	900	0	0.25	12	106±38	317	$0.62*10^{-3}$	0.33 ±0.003	1.43	0.1380
MG-SiC-10 0	1000	1	0.15	9	30± 7	569	$9.53*10^{-3}$	5.11 ±0.11	15.58	0.0789
MG-SiC-16 -1	900	0	0.05	5	56± 10	854	$8.08*10^{-3}$	4.33 ±0.06	8.07	0.0524

Table 3.4.2. Design of experiment table with primary results. Red marked lines are indicating the central values experiments, green are indicating the hadamard matrix experiments and the yellow one presents the «-1» experiment.

Chapter 4: Characterization of the deposited thin films

4.1 Microscopic characterization: structure and surface quality

Figure 4.1.1. presents the X-ray graphs for the undoped and doped poly-Sic. Two small peaks at 35°and 75°of 2θ, which they are associating with the 3C-SiC (111) plane and the 3C-SiC (222) plane respectively, are indicating a possible cubic formation of polycrystalline SiC. The pure XRD graph for the existence of a polycrystalline material, should display additional peaks of cubic formation of SiC, although their absence is not yet clearly explained. One possible explanation should be that the deposited material is highly oriented in the (111) direction. An advanced structural characterization like transmission electron microscopy would able to give significant information about the distribution of the grains orientation. However in our thesis our structural characterization methodology was limited. The additional peaks at 47° and 57°, are associated with the silicon crystalline planes (220) and (311) respectively, which they indicate the additional deposition of polycrystalline silicon, along with the poly-SiC. The decreased intensity of the Si peaks in the *in situ* chloride treated films confirms that the induced chloride species prevents the extensive formation of polycrystalline silicon. However an increase of the chloride treatment duration show increase of the polysilicon grains size. This is depicted by the increased intensity of the silicon peaks. The X-ray graph of the doped film indicates smaller peaks, due to the induced nitrogen atoms. This confirms the decrease of the overall crystallinity of the lattice in n-doping of polycrystalline SiC, due to the shrinkage of the lattice.

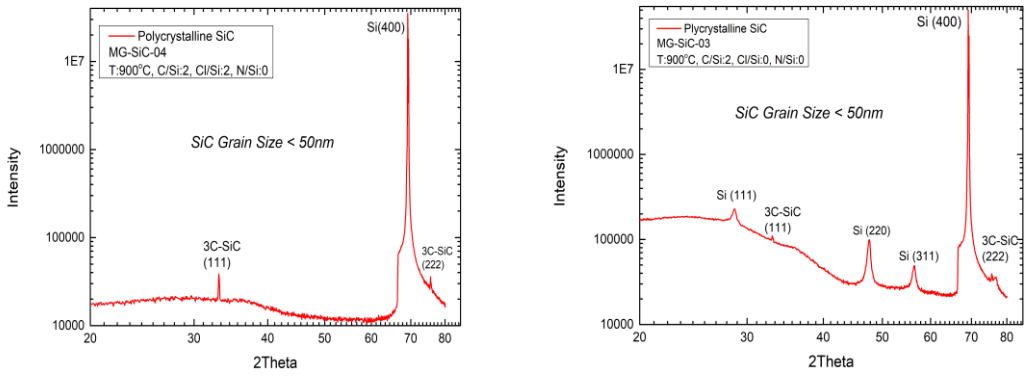

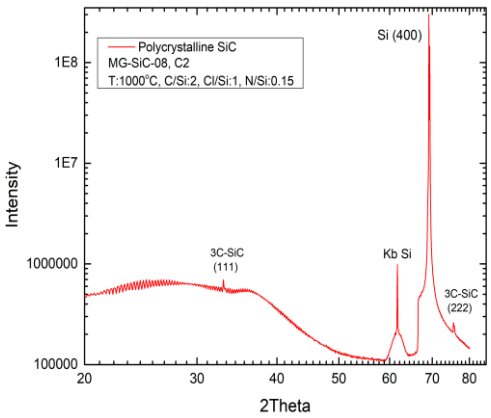

Figure 4.1.1.(Up-Left) XRD diffractogram of undoped poly-SiC under chloride ambience Cl/Si:2. Chloride treatment decreases the amount of the poly-Si grains deposited within the poly-SiC. (Up-Right) XRD diffractogram of undoped poly-SiC without chloride treatment. Polycrystalline silicon peaks indicate the deposition polysilicon grains within the poly-SiC. (Down) XRD diffractogram of n-doped polycrystalline SiC with chloride treatment. The reduced intensity of the SiC peaks are associated with a reduction in film's crystallinity caused by the induced nitrogen atoms.

The X-ray graphs (Figure 4.1.2.) of the DOE samples (Table 3.4.3) are similar showing no significant change between them. The two observable peaks are only those of 3C-SiC (111) crystal plane and the 3C-SiC of the crystal plane (222) respectively. The two peaks show no change on the intensity on varied temperature, which means that the average grain size is steady between 900^{o}C and 1100^{o}C. The silicon peaks are again completely vanished for the films that are chloride treated.

The small intensity of the SiC-related peaks signifies the growth of nanocrystallites below the 50nm average size. The grains size can be determined by the FWHM of the corresponding peak combined with the peak's intensity. With such grain size it is difficult enough to identify the reduction on crystallinity, since nanocrystallites tend to show very small changes on their structure and orientation. It is possible as well, that the *in situ* doping prevents the growth of large grains in this temperature range. The induced high amount of nitrogen surrounding the crystallites, create a shield around them, preventing them of growing more, while the next nanocrystallites tend to grow on top of them, repeating the growth-shield circle until the end of the deposition. This process is probably remains active for the chose ambient temperature range (900^{o}C – 1100^{o}C).Although that the chloride treatment has shown a direct increase of the grain size ([39]), it is not observable in our experiments, something that may be resulted by the low ambient temperature. It has been reported that grains above 20nm in size, can be achieved in 1300^{o}C temperature in a vertical cold wall system with silane and propane standard chemistry, while in our approach the temperature is far below this level ([47]).

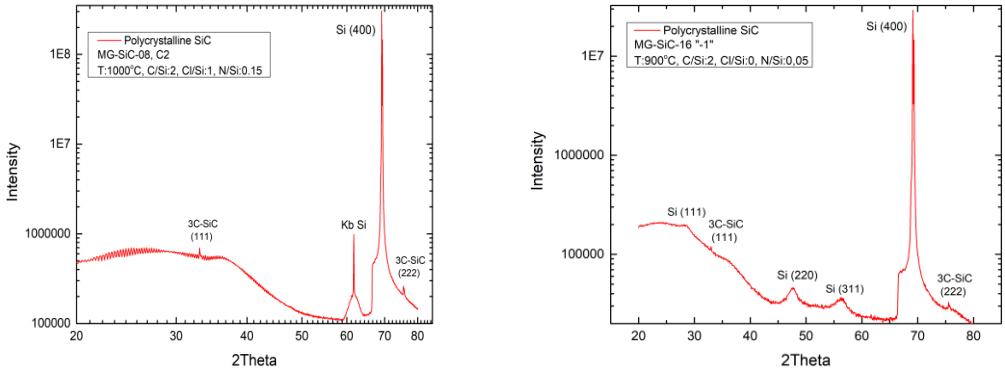

Figure 4.1.2. XRD graphs for the deposited thin films based on the DOE optimal conditions. (Left) XRD graph of C2 DOE experiment presents the possible existence of cubic silicon carbide 3C-SiC, with nanosize grains (<50nm). The absence of poly-Si line is featured to the absence of chloride respectively. (Right) XRD graph of the «-1» DOE experiment contains bands related with the poly-Si deposition within the 3C-SiC lattice.

Cross section Raman spectra of n-doped polycrystalline SiC is displayed in the Figure 4.1.3. Unfortunately, the measurements were very noisy. The broad band nearly on the 900cm^{-1} is associated with the convolution of three possible band modes TO and LO phonons of the 3C-SiC and the Si-N mode at 1046cm^{-1}. This overlapping between these two bands is a characteristic of low crystallinity and small grain size. In general broadening of Raman bands can occur in decreased grain size lattice. The strong peak on 490 cm^{-1} is similar with the TO phonon band of silicon at 520 cm^{-1}, although it can be also associated with the LA phonon mode in the Γ spot of the 3C-SiC Brillouin zone. The low overall intensity is resulted by the low thickness of the deposited layer.

A sharp peak nearly at 1136 cm^{-1} is associated with the N-H phonon band, which confirms the doping of the thin film and the embedded hydrogen into the lattice. Hydrogen trapping inside the crystalline lattice has also been reported in other previous thin film studies of SiC and SiN_3 ([45]), ([46]). The absence of G or D bands associated with the active Raman modes of C-C bond indicates that no formation of amorphous carbon sites or graphene sites is deposited.

Overall no significant change is observed on spectra related to the DOE films. Again this observation is correlated with the temperature range we are investigating. In such low temperature no big variations are expected, due to the nano size of the deposited grains. In the «-1» experiment (Table 3.4.3) peaks related to crystalline silicon are also observable. This comes in agreement with the XRD graph of the same experiment, confirming the existence of polysilicon grains within the poly-SiC lattice.

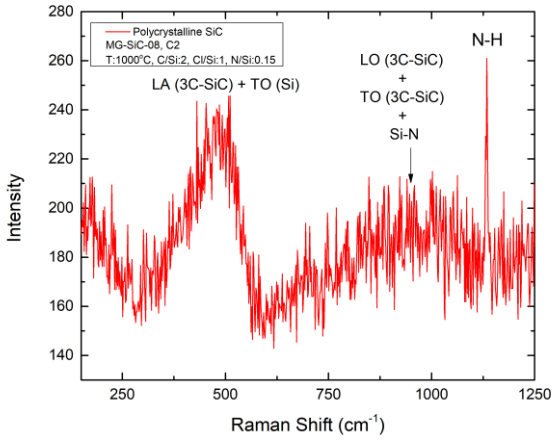

Figure 4.1.3. Cross section Raman spectrum of the deposited n-type poly-SiC of the DOE. The peak on 500 cm^{-1} Raman shift is possibly a convolution of TO mode of silicon LA phonon of SiC at Γspot of the Brillouin zone. The broad band is probably associated with the convolution of three specific bands the LO and TO bands of 3C-SiC and the Si-N stretching band. The excitation laser was set at 514nm and its power at 10mW.

The average surface roughness is strongly affected by the chloride ambience. Under chloride treatment the estimated surface roughness was 5 times lower than the untreated one. Figure 4.1.4. displays the root mean square of the surface roughness for the poly-SiC in terms of chloride treatment. It is clear that the chloride ambience prevents the extensive nucleation on top of the surface. In contrast it is observed that small valley-like trenched regions are formed, which are resulted by a possible etching of the passing chloride. These valleys are possibly shaped by a peeling of small pieces of SiC flakes. In contrast in the non-chlorinated film, the surface is consisting of sharp SiC columns, which are formed by intense nucleation with a pyramidal shape.

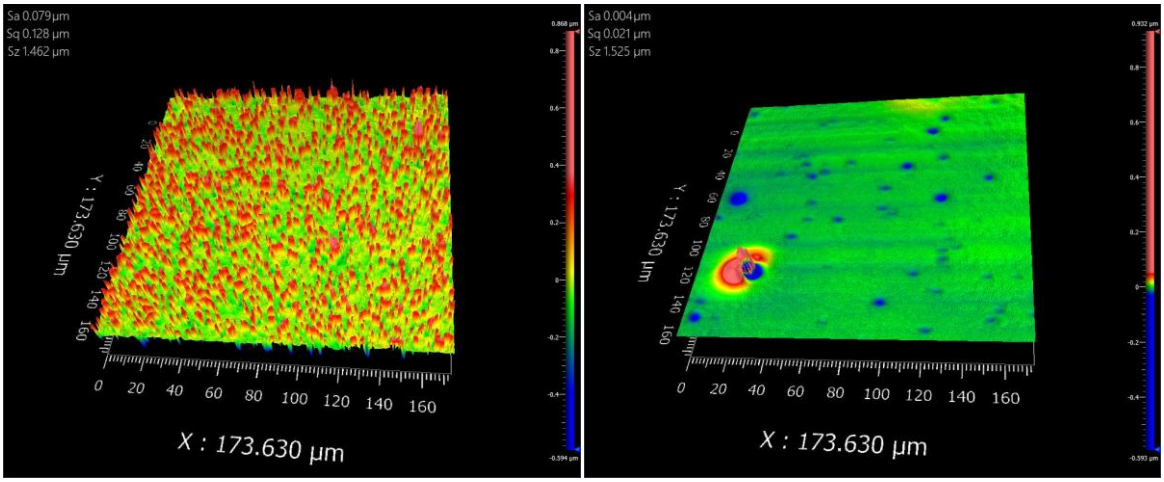

Figure 4.1.4. (Left) Root mean square (RMS),(Sq = 128nm) of average surface roughness of polycrystalline SiC, with Cl/Si:0. (Right) Root mean square of surface roughness (Sq = 21nm) of chloride treated polycrystalline SiC, with Cl/Si:2.

Based on the DOE analysis results (see chapter 3) the induced nitrogen exceeding the N/Si:0.05 value, reduces the residual stress, something that comes in contrast with previous studies of poly-SiC doping stress ([5]). However since all the growth conditions have

significant impact on the stress is difficult to determine the nitrogen mechanism on stress, ignoring the other two growth parameters. Temperature's effect on the other hand is consistent with previous studies, reporting that the increasing of temperature could lead to a higher growth rate, which concludes to a reduction of the residual stress ([40]), ([41]), ([42]). However it is yet unclear if temperature has a direct impact on the chloride or nitrogen mechanism. Chloride amount in contrast is proportional to the resulted stress, since its strong etching reduces significantly the final formatted thickness that directly associated with the corresponding residual stress.

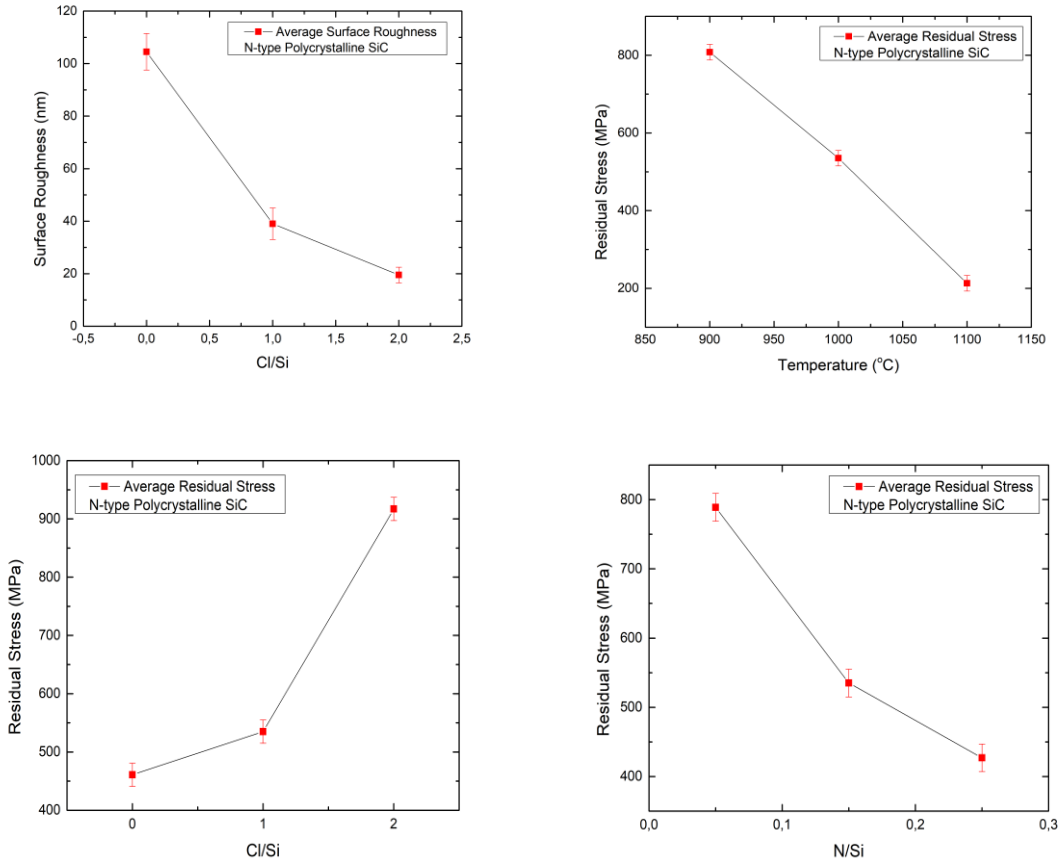

Figure 4.1.4. (Left-Up) Root means square of the surface roughness vs. the ratio Cl/Si, of DOE poly-SiC thin films. (Right-Up) Temperature vs. residual stress of the DOE poly-SiC thin films. (Left-Down) ratio Cl/Si vs. residual stress of DOE poly-SiC thin films. (Right-Down) ratio N/Si vs. residual stress of DOE poly-SiC thin films. Error bars are consisting the standard deviation of each average measurement.

In our approach the films are presented as tensile, since they exhibit positive stress. The residual stress is ultimately measured at room temperature by optical profilometry. The tensile stress is attributed probably by a variety of reasons, both macroscopically and microscopically.

Macroscopically the corresponding stress could be possibly associated with the lattice shrinkage caused by the induced nitrogen atoms and the non uniform deposition of the film on top of the substrate. Thermal stress generated during the growth and the cooling process is probably the main contributor, based ultimately on the average temperature gradient between the room temperature and the growth temperature taking also account the thermal properties of the grown layer and the substrate. The lower thickness additionally with the most of it to

deposited directly in the middle of the wafer, creates a stress gradient, between the center and the planar sides of the film. This gradient creates a slight up bending of the sides, while the film/substrate system reshaped into a trench-like geometry (Figure 2.2.1).

This bending is microscopically associated with the thermal coefficients of SiC and Si. Because the thermal expansion coefficient is of SiC is higher than Si, the thermal stress generated in the film is tensile, after the substrate is cooled to room temperature. The thermal stress can be controlled by choosing a substrate material with proper thermal coefficient of expansion. In addition, intrinsic stress is also a significant reason of tensile stress, caused possibly by grains boundaries distribution, some trapped species inside the lattice like hydrogen or others non-stoichiometric compounds and the preferred growth orientations ([41]).

4.2. Macroscopic characterization: Electrical and Electrochemical performance

The electrical resistivity depends on the N/Si ratio (Fig. 4.2.1). The resistivity response experiences a rapid decrease from the un-doped sample until the N/Si:0.05 value. This resistivity gap has been observed many times in previous studies of n-doped poly-SiC ([5]), ([43]). When the N/Si ratio value is further increased the resistivity experiences a slight increase but still remains under 1 Ω*cm. Figure 4.2.1. displays the resistivity response for various values of N/Si ratio. Since a reduced in the film's crystallinity is expected, the amorphization is probably enhanced with the over doping of SiC lattice with nitrogen atoms. By constantly offering nitrogen into the lattice, even more Si-N bonds are formed, resulting in an even small average lattice constant, since the Si-N bond length is smaller than the one of Si-C bond.

The over shrinkage of the film, leading to an enhanced amorphization around the nitrogen sites, than by an increase of the resistivity. However this increase is low enough, consisting an attribute of the physical limit of the semiconductor to the band structure modulation. The dopants can either occupy shallow or deep levels within the forbidden gap. Either case can form a new electronic energy band, in between the conduction and the valence band, as long as the amount of the dopant atoms is big enough to allow so. When this electronic band is depleted from dopant atoms the electronic band structure cannot change further on and thus it cannot affect the corresponding sheet resistivity. Then the sheet resistivity is dependent only by the crystallinity of the lattice itself. Thus it is relevant to assume that within the range of N/Si value [0.05-0.25] the only effect on the resistivity arises directly from the decrease in the film's overall crystallinity.

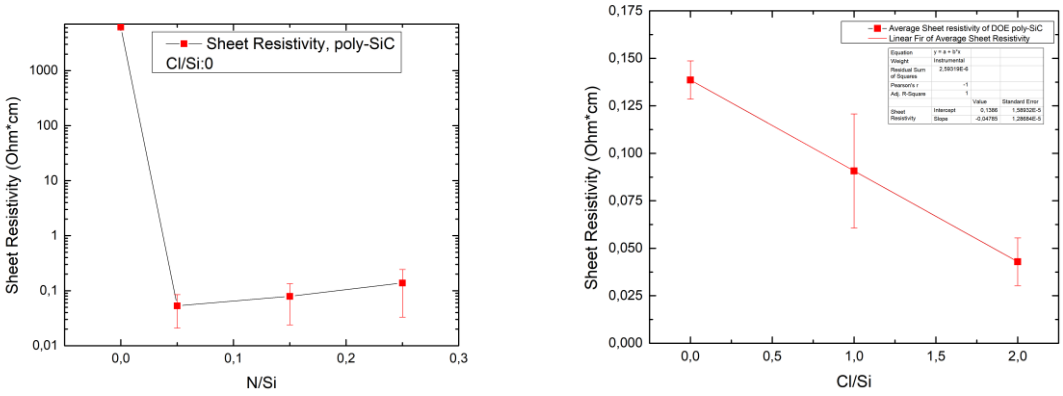

Figure 4.2.1.(Left)Electrical Resistivity resistivity of n-doped poly-SiC thin film vs. N/Si ratio in the gas phase.Cl/Si:0 value indicates absence of chloride during the thermal growth of the deposited thin film. (Right) Electrical resistivity vs. the ratio of Cl/Si in the gas phase. Both graphs are based in the experimental results on behalf of DOE technique.

The resistivity can also be modulated by chloride (Figure.4.2.1.). Both in the calibration test and in the DOE experiments, the chloride grown layers, exhibit significant lower levels of resistivity. Interestingly the average resistivity shows a fully linear relationship with the Cl/Si precursor ratio. This behavior is related to the effect of chloride to the resulted surface roughness. These results could be explained by the roughness induced resistivity phenomenon ([38]), ([44]). A given sheet resistivity should be arise from the reduced mobility of the free carriers in the geometrical space of the surface. Island like nucleation or pillars can work as intense scattering sites for the conductive carriers, electrons. Since the scattering in semiconductors can be described as a quantum process, the scattered carrier should end up on an available quantum bound state.

In rougher surfaces the amount of electron scattering sites, which impede the movement of free carriers is significant larger than in smoother surfaces. The scattering is a result of the collision between the free carriers and possible surface defects or vacant sites, which can be occur in a polycrystalline surface formation ([38]). Scattering sites can also been observed in very smooth surfaces, as planar surface defects or crystallites orientation mismatches. However the amount of the available quantum states is significantly reduced and thus the incoming carriers are ignoring many of the possible scatterers. Eventually the scattering probability is reduced, leading to an increase in the overall mobility of the conductive carriers on top of the surface. Thus the reduction of the scattering sites is decreasing along with the corresponding resistivity with an extensive *in-situ* chloride surface treatment of the deposited thin film. The roughness induced resistivity has also been reported in many previous studies of conductive thin films like Cu and W wires, with the analogous results ([38]), ([44]).

The CV data are displaying a capacitive behavior with the electrolytic ions. The hysteresis circle is indicating in most of films an anodic resistor-capacitor (RC) charging ramp until the current reaches a plateau value and remains almost steady until the voltage scan limit, where the next electric flux is caused by the potentiostat, scanning the opposite direction of potential, leading in a cathodic RC charging ramp that follows a similar current response. The charge storage capacity, pure capacitance and the charge delivered per phase can be estimated, within the hysteresis circle in a slow sweep rate (~50mV/s) ([31]). Results

are displayed by the normalized area (~0.75cm^2) of the poly-SiC electrodes (Table 3.2.2). The charge storage capacity varies between 1-15 mC/cm^2 and the charge delivery per phase varies within the range of 1-20 μC. The average capacitance varies between the 1-8 μF. Similar values of capacitance have also been observed in previous doped polycrystalline SiC studies deposited by PECVD technique ([9]).

Figure 4.2.2. displays the hysteresis circle of three explicit samples of the DOE poly-SiC films. Judging from the three hysteresis circles, the charge injection for the electrodes is strictly capacitive. The absence of pseudo-capacitance is excluding any possible adsorption effects on the electrodes' surface. Clearly the C1 shows the steadiest capacitive behavior. The H1 shows poor capacitive response, storing the lowest charge of them three. The «-1» suffers from an increased current, that could be associated with an oxidation, Faradaic current that it is initiated after the 0.3V potential value. This reduction of the anodic water window could be caused, most possibly, by the existence of the poly-Si nanocrystalles within the poly-SiC, since all of the optimal conditions don't show a descent effect to the electrochemical measured values based on the DOE analysis. The participation of poly-SiC fused with poly-Si affects obviously the electrochemical properties of the electrode, while they don't have specific change on the charge storage and delivery. Since the poly-Si has lower band gap than the poly-SiC, it is a good provider of free carriers, while the shallow and deep level nitrogen donors, can be ionized easily enabling the higher available amount of free carriers close to the electrode/electrolyte interface. In addition the absence of chloride could result in a Si-rich columns on top of the film's surface. The Si-rich surface combined with the features of poly-Si that mentioned before is probably responsible for the change in the electrochemical response. An extensive study should suggest that the electrochemical response is associated with the variation of the Si percentage on the film but for the moment is not clear. For this further experimenting is required in terms of surface analysis and electrochemical testing. The cathodic scanning displays only the charging rump without any Faradaic current. The C1 and H1 show a hysteresis circle without compromising their water window in this chosen potential range. This could suggest that the growth conditions based on the C1 and H1 electrodes are possible the best for a neural interface application. The C1 electrode shows the highest amount of CSC exposing the best optimal conditions for a descent deposited film for neural stimulation applications.

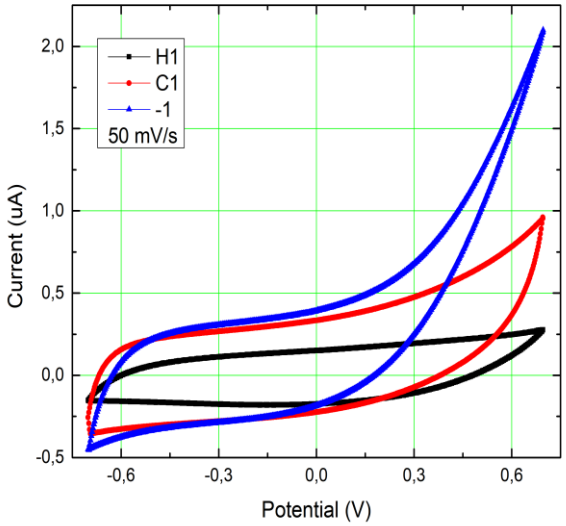

Figure 4.2.2. Hysteresis circle for H1, C1 and «-1» experiments. All of the CV data were acquired using a scan rate of 50mV/s and the Pt water window as scan range (-0.7V, +0.7V). All of the samples were shown a background current at (V=0) between 0.2 and 0.5 μA for both anodic and cathodic scanning.

Electrochemical measurements on PBS buffer solution were also performed for various related material that are known for their use in neural interfaces applications (Figure 4.2.3). Epitaxial 4H-SiC and N-doped Si wafer show a very small charge ramp with an overall steady capacitive behavior, which is very usual in high crystalline materials. TiN shows the biggest charging of the electrostatic double layer. The n-doped polycrystalline SiC displaying bigger charging than the epitaxial materials, with symmetrical anodic and cathodic response. The polycrystalline phase of SiC enables the storage of trapped charge in the grain boundaries of the crystalline orientation. Due to the existence of grain boundaries, the carrier transport behavior of the polycrystalline material is departed from the single crystalline counterpart. The grain defects and the rougher surface, which has more available free bound states as mentioned before, are enabling the trapping of free carriers, which can increase the overall capacitance of the active surface. Thus this enhances the capacitive current response of the polycrystalline SiC, as long as the charging of the Helmholtz layer is bigger, compare to the epitaxial film.

The non pure charging process of the polycrystalline SiC indicates an RC equivalent circuit that includes a parallel resistance R_p to the capacitive element. The overall equivalent circuit usually consists of the capacitance of the electrostatic double layer (C_H) and the Electrolyte resistance (R_F). The R_p component is actually a combination of two additional components that exist exclusively in the semiconductors electrochemistry ([49]). The semiconductor-electrolyte interface behaves similar with the semiconductor/metal, Schottky junction. At the equilibrium state this interaction leads to a fixation of the Fermi level and a bending of the conduction and valence band. In this case the surface of semiconductor is depleted by the minority carriers, forming the space charge region (or layer). The additional components on the equivalent circuit are the space charge capacitance (C_{sc}) and a resistive component that corresponds to the speed of the surface charge state (R_{ss}). These two elements are derived directly from the space charge region formation and delay the full charge of the

electrostatic double layer that is very common to the non-epitaxial semiconductors. As a result, it displays a higher charge storage capacity than the epitaxial counterpart and the pure doped silicon.

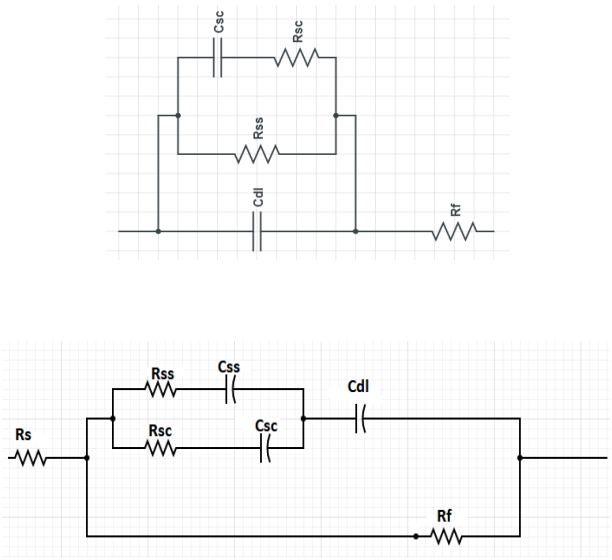

Figure 4.2.3. (Up) Equivalent circuit of Cyclic voltammetry for semiconducting polycrystalline SiC. Cdl indicates the double layer capacitance, while Csc indicates the surface charge capacitance. The resistive components are the electroclyte resistance Rf, the charge surface resistance, Rcs and the surface state resistance Rss. (Down) Randles circuit of Electrochemical Impedance Spectroscopy for the semiconducting polycrystalline SiC. One additional capacitive component, the surface state capacitance, Css, is also presented, arising by the alternative current capacitive resistance, during the impedance response.

That property could suggest the polycrystalline SiC as a suitable material for neural recording. The higher available capacitance also suggests that the polycrystalline material should also be used appropriately for neural stimulation causes.

Electrochemical impedance response was also recorder for various electrochemical materials(Fig. 4.2.4). N-doped polycrystalline SiC exhibits lower impedance response compare to its epitaxial counterpart. N-doped silicon wafer ($\rho_{n\text{-}Si}$=0.0012 Ω*cm) and TiN show the lowest impedance response, as these materials have been reported many times before as promising materials for neural interfaces, based on their low electrochemical impedance. Rather than being nitrogen doped the polycrystalline SiC maintains high impedance in general. This should be corresponded to the average grain size of the lattice structure. The wavy impedance response should be connected with the average space charge and surface state capacitances. The impedance response is directly connected with the overall capacitance of the material. This fluctuation of impedance is probably related with a small space charge and surface state capacitance ([49]). The low capacity indicates a large space charge layer accompanied by a small population of corresponded carriers close to the electrolyte interface. The surface state capacitance is probably remains small since the high amount surface grain boundaries, could trap extensive charge (electrons), causing a higher impedance on the carriers movement during the surface state change, that caused by the AC voltage shift. Randles circuit (Figure 4.2.3) displays the three capacitive elements of them that they contribute to the impedance response. Since these two capacitances are smaller that

the electrochemical double layer capacitance, they determine the total influence of the overall capacitance, while they are in a serial configuration.

The grain size is possible connected also with the induced resistance of the surface state. The amount of grain boundaries and intra grain defects is bigger in small size grains, and so does the amount of trapped charged carriers. The low amount of available conductive carriers is linked with a weak depletion of the electrode's surface. This phenomenon is probably resulting to an enhanced surface state resistance. Space charge capacitance can also affect the impedance response. Similar with the enhanced surface state resistance the overall amount of free carriers facing the electrolyte is relatively small, inside space charge layer. Therefore the corresponding space charge layer is relatively large, resulting to a small space charge capacitance as well. Thus the corresponding impedance response is relatively high. The reduced crystallinity is also affecting the impedance response, since amorphous regions are initiating the impedance response, throughout the bulk phase of the thin film.

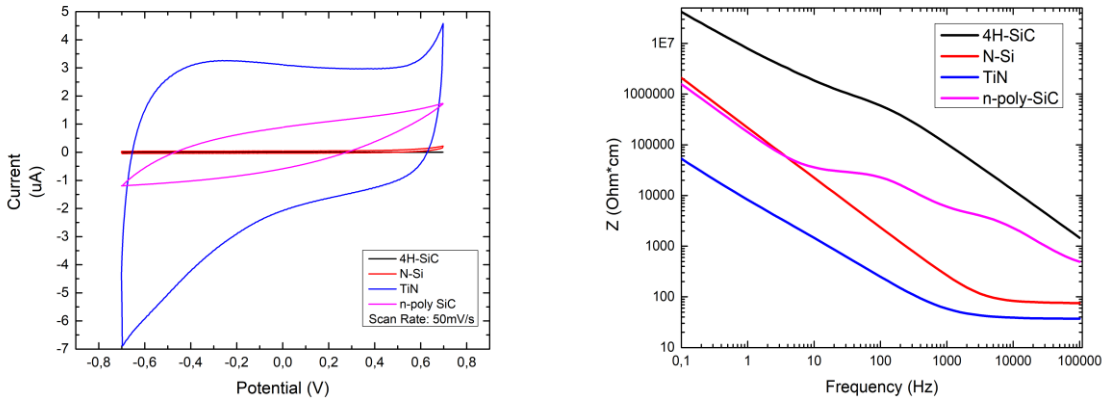

Figure 4.2.4. (Left) Hysteresis circle for various semiconducting and metallic materials. Scan range is the commercial platinum water window (-0.7V, +0.7V). (Right) Impedance response for various materials electrochemical materials. Both experiments were performed in a PBS buffer solution (pH:7.4).

Chapter 5. Summary and Future Work

5.1 Summary

Polycrystalline SiC thin films can successfully grow using the LPCVD, with adjusted properties for brain implantable applications. The average properties are directly controlled by the optimal conditions of the deposition. The standard chemistry of silane and propane allows the descent growth of polycrystalline 3C-SiC both un-doped and n-doped films, in the temperature range of 900^{o}C – 1100^{o}C.

The accompanied Cl_2 gas can successfully decrease the average surface roughness. Also it can perform an intense etching process in high flow rates, which has a direct impact in the reduction of the resulted thickness.

N-doping can be performed by *in situ* ammoniaNH_3 gas inlet, which is a good provider of nitrogen, doping atoms.

Polysilicon grains are possibly grown within the poly-SiC lattice that can participate in the properties of the deposited film. The elimination of them can be achieved with the induced chloride gas, due to the thermodynamically favorable Si-Cl bond, instead of the Si-Si bond, for temperatures above 900^{o}C.

The residual stress is affected intensively by the induced chloride species. The average thickness controlled by the strong chloride etching, along with the shrinkage of the lattice, due to the induction of nitrogen atoms, determine the average residual stress, which is found to vary between 200MPa – 1GPa.

Electrical resistivity as low as some mΩ*cm can be achieved with direct nitrogen doping and with chloride surface treatment. The ammonia as a nitrogen provider, and the surface smoothing by chloride, allow the addition of free carriers and the reduction on the amount of free electron scattering sites, enhancing the overall conductivity of thin film.

The electrochemical performance shows to be almost steady no matter the different level of doping of induced, the ambient temperature or the chloride treatment. This is highlighted, due to the average grain size, which is estimated to be under 10nm. The surface intra-grain defects and the diffused grains boundaries affecting deeply the capacitance and the mobility of the free carriers in the electrode/electrolyte interface. The nanosize grains are most probably responsible also for the high impedance response as the response in the AC current perturbation is poor due to the high charge state resistance.

5.2 Future Work

5.2.1 Improving the crystallinity and grains size of poly-SiC

To have a more reliable based material for the fabrication of microelectrodes, we must first improve the crystallinity and the grain size of the individual crystallites. Deposition of un-doped polycrystalline SiC on increased ambient temperature (~1300^{o}C) in a vertical cold-wall system can show intense growth of large size crystallites, since it has been reported in previous deposition studies ([50]). A two step deposition can be performed, starting with a small carbonization process at 1000^{o}C for 90s using propane, with a following step of introducing silane into the reactor for almost 1 hour. Another possibility is to keep the

experiment as an one process deposition in 1300^{o}C for 1 hour long, with a varied C/Si ratio. Chloride ratio Cl/Si could also be taken into account in the grain size modulation or modification of crystallinity.

5.2.2 Investigating the doping the microscopic doping mechanism for the poly-SiC

As long as we achieve a better crystal quality and a descent size of crystallites (~μm) than in our current approach, we can investigate the microscopic doping mechanism with the introduction of ammonia into the CVD reactor. The doping can be performed in different cases of ammonia, changing the flow rate but limiting the ratio of N/Si below 0.05. In general the doping investigation should be more stable after determining the appropriate C/Si and Cl/Si values for a good quality un-doped polycrystalline material. The procedure could be either *in situ* or by single nitrogen treatment on top of the un-doped deposited film. The confirmations of the nitrogen existence can be identified by either Raman spectroscopy, by the Si-N band or by XRD showing a lower crystallinity compare to the un-doped counterpart. Trapped hydrogen was detected also by Raman, due to the N-H bond. Normally the presence of hydrogen is undesirable, since the bonded hydrogen probably passivates N and not allow the nitrogen atoms to participate in doping effectively. Thus a study on the variation of N-H Raman peak with the corresponding resistivity could give significant information of the doping efficiency. In addition the trapped hydrogen could be avoided, by decreasing the number of the N-H bonds, performing a post-deposition annealing, enhancing the doping of the thin film.

We aim for the evaluation of the doping effect on the microscopic properties of the material, like the change in the band structure, the number of the free conductive carriers and their mobility by Hall Effect measurements and many macroscopic properties like the resistance, the sheet carrier density and the majority carriers concentration by the Van der Pauw technique. Thermal dependent electrical conductivity and resistivity can be estimated by a four-point probe technique and simple I-V electrical measurements.

Mechanical properties can also be estimated depending on the nitrogen amount, since the chloride amount should remain overall steady in order to eliminate the etching variation effect from the experimental procedure. Thus the stress will be directly N/Si value dependent. In that case we can examine the stress gradient based specifically on the doping mechanism.

5.3.2 Investigating the electrochemical performance of macro and microelectrode poly-SiC.

After find the best possible optimal conditions for the growth of conductive poly-SiC films, the next step is to improve their electrochemical performance. Some attempts to use the black platinum electroplating technique, in order to decrease the impedance response, have been reported in the past. Other option could be to use polymeric coating of PEDOT:PSS in order to increase the capacitance response, or to investigate the effect of induced surface roughness capacitance.

Next the fabrication of microelectrode array will give a better understanding of the electrochemical performance, since it has been shown that the overall device tends to express different properties in the final application than the pure material itself. The microelectrodes can be fabricated with different geometries with respect the minimization of the foreign body

response and the enhancement of the charge storage capacity for neural stimulating and recording reasons.

5.3 Special Thanks

Approaching to the end of this master program, I would like to thank all the people that convolute for the accomplishment of this project. I would like to give my thanks to the ANR organization and the Grenoble-INP institution for funding my research and support my work. Many thanks should be also given to the associated researchers from SIMaP and the related materials that contribute in the SiCNeural project. Additional thanks are given also to the University of Crete faculty members of the Photonics and Nanoelectronics program, along with the Microelectronics research team of the FORTH-IESL institution of Crete.

References

[1]. Donoghue JP, Bridging the brain to the world: a perspective of neural interfaces . *Neuron* , pp. 60:511-521.,2008

[2]. (2009, June 09). Seth J. Wilks, Poly(3,4-ethylenedioxythiophene) as a micro-neural interface. *Frontiers in Neuroengineering* , pp. Volume 2, Article 7 .

[3]. Xiao-Fu, Mechanical properties and morphology of Polycrystalline 3C-SiC films deposited on Si and SiO2 by LPCVD*Materials Research Society symposium, 2004* Vol. 795

[4]. Richard A. Normann, The Utah Electrode Array: a recording structure for potential for potential brain computer interfaces. *Electroencephalography and Clinical Neurophysiology* , pp. Volume 102, Issue 3, 228-239., 1997

[5]. Fang Liu, Growth and characterization of nitrogen-doped polycrystalline 3C-SiC thin films for harsh environment MEMs applications. *Journal of Micromechanics and Microengineering, 2010* .

[6]. Xiao Yang, Bioinspired neuron-like electronics. *Nature Materials* , pp. https://doi.org/10.1038/s41563-019-0292-9., 2019

[7]. Diaz-Botia et al, 2017, J. Neural Eng. pp. DOI: 10.1088/1741-2552/aa7698.

[8]. Evans K. Bernardin, Demonstration of a Robust All-Silicon-Carbide Intracortical Neural Interface . *Micromachines* , pp. 9, 412; 2018 doi:10.3390/mi9080412.

[9]. Xao Zhuang, Electrochemical Properties and Applications of Nanocrystalline, Microcrystalline and Epitaxial Cubic Silicon carbide. *Applied Materials and Interfaces* , 2015 p. DOI: 10.1021/acsami.5b02024.

[10]. Brain Computer Interfaces: Definitions and principles, Wolpaw JR. *Handbook of clinical Neurology* , pp. Vol 68, 2020 .

[11]. *Mind, Brain and adaption in the nineteenth century, Young RM (1990).* Oxford University Press .

[12]. Memory in neuroscience, Wolpaw JR, rhetoric versus reality . *Behav. Cong. Neuroscience Rev* , pp. 1:130-136.,2016

[13]. Polikov V.S., Response of brain tissue chronically implanted neural neural electrodes. *J. Neuroscience Methods* , pp. 148, 1 -18 .,2016

[14]. Rousche P.J., Chronic recording capability of the Utah Intracortical Electrode array in cat sensory cortex. *Journal of neuroscience Methods* , pp. 82:(1), p:1-15., 1998

[15]. Oxley TJ, Minimally invasive endovascular stent-electrode array for high-fidelity, chronic recordings of cortical neural activity . *Nature Biotechnology* , pp. 34:320-327.,2016

[16]. John E. Ferguson. *Sensors and Accurators* , pp. A 156, 388-393., 2009

[17]. S. E. Saddow, 3C-SiC on Si: A bio and hemo-compatible material for advanced nano-bio devices. *Nanotechnology Materials and Devices Conference, IEEE* , pp. 49-53., 2014

[18]. C. L. Frewin, Silicon carbide Neural Implants: in vivo neural tissue reaction . *Neural Engineering, 6th International Conference IEEE/EMBS* , pp. 661-664., 2013

[19]. E. Bernardin, Demonstration of an all-SiC neuronal interface device. *MRS Advances Spring Meeting* 2018.

[20]. E. K. Bernardin, Demonstration of a Robust All-Silicon-Carbide Intracortical Neural Interface. *Micromachines* , pp. 9,x;., 2018

[21]. M. Wijensudara, Nitrogen doping of polycrystalline 3C-SiC films grown using 1,3-disilabutane in a conventional LPCVD reactor. *Journal of Crystal Growth* , pp. 259, 18-25., 2002

[22]. Electrical Characterization of n-Type Polycrystalline 3C-Silicon Carbide Thin Films deposited by 1,3-Disilabutane. *Journal of Electrochemical Society* , p. 153 (6)., 2006

[23]. *Henrik Pedersen, Chloride-Based Silicon Carbide CVD.* Linköping Studies in Science and Technology, 2008, ISBN: 978-91-7393-752-8.

[24]. Scanning Electron Microscopy . *Nanoscience Instrument* .

[25]. Optical Profilometry . *Nanoscience Instruments* .

[26]. Optical Profilometers . *Zygo Instruments* .

[27]. M. Ardigo, Stoney Formula: Investigation of curvature measurements by optical profilometer. *HAL open science*, 2014

[28]. Sheet Resistance Measurements on Thin Films . *Ossila: Enabling Materials Science* .

[29]. Linear sweep and Cyclic Voltammetry. In *Cambridge University, Chemical Engineering department, Teaching Notes .*

[30]. A practical Beginner's guide to Cyclic Voltammetry, Elgrishi N. *Jr. Chem. Edu.* , pp. 95,197-206., 2018

[31]. Neural Stimulation and Recording Electrodes, Cogan S. *Annu. Rev. Biomed. Eng.* , pp. 10:275-309., 2009

[32]. *Bernardin K.Evans, Demonstration of a Monolithic-Silicon Carbide (SiC) Neural Devices.* Tampa, Florida : University of South Florida, 2018 .

[33]. *Modern Raman Spectroscopy, Ewen Smith.* John Wiley and Sons Ltd., 2005.

[34]. *Introductory Raman Spectroscopy, J. R. Ferraro, K. Nakamoto, C.W. Brown.* Elsevier, Second Edition (2003) .

[35]. Exploring Non-Linearities of Carbon-Based Microsupercapacitors from an Equivalent Circuit Perspective, Danupol Boonpakdee. *Journal of Materials Chemistry* , p. DOI: 10.1039/C8TA01995A., 2018

[36]. The Electrical Double layer *Undergraduate Teaching Notes, University of Cambridge, Department of Chemical Engineering and Biotechnology*

[37]. Numerical Study of SiC CVD in a vertical cold-wall reactor*Computational Materials Science 24 (2002) 520-524*

[38]. Youqi Ke, Resistivity of thin Cu films with surface Roughness *Physical Review B* 79, 155406, 2009

[39]. R. Boichot, Epitaxial Gorwth of AlN on (0001) Sapphire: Assesment of HVPE Process by a Desing of Experiments Approach*Coatings* 7(9), 136, doi: 10.3390/coatings7090136,2017

[40]. Fu, Low stress polycrystalline SiC thin films suitable for MEMs applications*Jounral of electrochemical society* 158 (6) H675-H680, 2011

[41]. Fu, Residual stress characterization of polycrystalline 3C-SiC on Si(100) deposited from methylsilane *Journal of Applied science* 106, 013505; doi: 10.1063/1.3157184, 2009

[42]. Boo, Growth of cubic SiC Films using 1,3-Disilabutane *Chem. Matt.* Vol. 7, No. 4, 1995

[43]. Zhang, Electrical characterization of n-type polycrystalline 3C-Silicon carbide thin films deposited by 1,3-Disilabutane *Journal of Electrochemical Society* 153 (6), G548-G55, 2006

[44]. Zheng, Surface Roughness dependence of the electrical resistivity of W(001) layers *Journal of Applied Physics* 122, 095304,2017

[45]. Liu, Applications of UV-Raman Spectroscopy to Microelectronics Materials and Devices *Characterization and Metrology for ULSI Technology Conference, 2003*

[46]. Bandet, Nitrogen bonding environments and local order in hydrogenated amorphous silicon nitride films studied by Raman spectroscopy *Journal of Applied Physics* Vol. 8, N. 5, 1999

[47]. Zorman, Characterization of polycrystalline SiC films grown by atmospheric pressure chemical vapor deposition on polycrystalline Si *Journal of Materials Research* Vol. 13, No. 2, 1999

[48]. G. Chichignoud, Chlorinated Silicon Carbide CVD revisited for polycrystalline bulk growth. *Science Direct, Surface and Coating Technology* , pp. 201, 8888-8892, 2007.

[49]. P. Allongue, Band-Edge Shift and surface charges at illuminated n-GaAs/Aqueous Electrolyte junction: Surface state analysis and stimulation of their Occupation Rate. *Journal of Electrochemical Society* , pp. Volume 132, Issue 1, Pages 42-44.,1985

[50]. C.A.Zorman, Characterization of polycrystalline silicon carbide films grown by atmospheric pressure chemical vapor deposition on polycrystalline silicon. *Journal of Materials Research* , pp. Vol. 13, No. 2., 1999